

Use Authorization

In presenting this thesis in partial fulfillment of the requirements for an advanced degree at Idaho State University, I agree that the Library shall make it freely available for inspection. I further state that permission to download and/or print my thesis for scholarly purposes may be granted by the Dean of the Graduate School, Dean of my academic division, or by the University Librarian. It is understood that any copying or publication of this thesis for financial gain shall not be allowed without my written permission.

Signature _____

Fatima Khokonova

Date _____

**SAAM II Predictions based on ICRP 78 Systemic Model
coupled to NCRP 156 Wound Model for Plutonium**

By

Fatima Khokonova

A thesis

submitted in partial fulfillment

of the requirements for the degree of

Master of Science in Department of Nuclear Engineering and Health Physics

Idaho State University

Fall 2014

To the Graduate Faculty:

The members of the committee appointed to examine the thesis of Fatima Khokonova find it satisfactory and recommend that it be accepted.

Dr. Richard Brey

Major Advisor

Dr. Jason Harris

Committee Member

Dr. DeWayne Derryberry

Graduate Faculty Representative

ACKNOWLEDGEMENTS

Foremost, I would like to express my special appreciation and gratitude to my major adviser Dr. Richard Brey for his help, encouragement, motivation and immense knowledge. This thesis would not have been possible without his support and patience. He has also provided insightful discussions about the research during our internal dosimetry group meetings.

Besides my advisor, I would like to thank the member of my committee Dr. Jason Harris for serving as my committee member and being a great instructor in one of my favorite classes. I am also very grateful to Dr. DeWayne Derryberry for being a Graduate Faculty Representative for my thesis, for providing me advice and suggestions on statistics.

I will be thankful to my former research advisor Dr. Valeriia Starovoitova for her help and teaching while she was a postdoc at Idaho Accelerator Center. I would like to thank Dr. George Tabatadze for his assistance and being a great teacher in four classes I have taken during my studying. I would like to thank Kevin Claver the supervisor of the Environment Assessment Laboratory (EAL) for providing me advice and support. I thank all of my friends for providing support and friendship for the entire time I was at ISU.

A special thanks to my family. Words cannot express how grateful I am to my mother and my uncles for all of the sacrifices that they have made on my behalf and for supporting me during the hardest times.

TABLE OF CONTENTS

List of Figures	vii
List of Tables	ix
Abstract	x
Chapter 1 : INTRODUCTION	1
1.1. The purpose of the study	1
Chapter 2 : LITERATURE REVIEW	3
2.1. Plutonium	3
2.2. Biokinetics of Plutonium	5
2.2.1. ICRP 78 Systemic Model for Plutonium	5
2.2.2. NCRP 156 Wound Model for Plutonium	9
2.3. Retention and Translocation of Systemic Pu	13
2.3.1. Deletion from the blood	14
2.3.2. Distribution and retention in the skeleton	15
2.3.3. Distribution and translocation in the liver	16
2.3.4. Soft Tissues	16
2.3.5 Excretion	17
Chapter 3 : MATERIALS AND METHODS	18
3.1. SAAM II	18
3.2. Methods of Analysis	19
3.3. Total Objective Function	23
3.4. The Akaike Information Criterion (AIC) and the Schwarz-Bayesian Information Criterion (BIC)	25
Chapter 4 : RESULTS AND DISCUSSIONS	27
4.1. SAAM II Prediction based on ICRP 78 Systemic Model coupled to NCRP 156 Wound Model	27
4.2. Optimization of the Transfer Rates suggested in the ICRP 78 Systemic Model and NCRP 156 Wound Model for Plutonium	45
Chapter 5 : SUMMARY AND CONCLUSIONS	56
5.1. Summary of Results	56

5.2. Future Work	57
Bibliography	58

List of Figures

Figure 1: ICRP 78 Systemic model for Plutonium	7
Figure 2: NCRP general wound model	9
Figure 3: Wound Model for Injection of Soluble Substances	11
Figure 4: Diagram of the compartments used in the model and the direction of movement of Pu among these compartments	14
Figure 5: Name of the transfer coefficients	18
Figure 6: SAAM II main window with four main areas: the menu bar, the toolbar, the toolbox, and the drawing canvas	19
Figure 7: Schematic illustration of the ICRP 78 systemic model coupled to NCRP 156 wound model for plutonium in SAAM II	20
Figure 8: Input Window for Initial Amount of Activity in SAAM II	21
Figure 9: The data window in SAAM II	22
Figure 10: Parameter window in SAAM II	23
Figure 11: Case C95F sacrificed 8 days after injection	28
Figure 12: Case C103F sacrificed 20 hours after injection	29
Figure 13: Case C77F sacrificed 2 hours after injection	30
Figure 14: Case C108F sacrificed 18 hours after injection	31
Figure 15: Case C103F sacrificed 20 hours after injection	32
Figure 16: Case S114F sacrificed 7 days after injection	33
Figure 17: Case C145M sacrificed 7 days after injection	34
Figure 18: Case C95F sacrificed 8 days after injection	35
Figure 19: Case C131F sacrificed 56 days after injection	36
Figure 20: Case R186M sacrificed 103 days after injection	37

Figure 21: Case C106M sacrificed 106 days after injection	38
Figure 22: Case C166M sacrificed 106 days after injection	39
Figure 23: Case C80F sacrificed 1,100 days after injection	40
Figure 24: Scatter plots of the retention fractions in Liver and Skeleton for SAAM II prediction and measured values	44
Figure 25: Case C108F sacrificed in 18 hours after injection. Initial predictions and final solutions after optimization of transfer rates	46
Figure 26: Case C103F sacrificed in 20 hours after injection. Initial prediction and final solution after optimization of transfer rates	47
Figure 27: Case C145M sacrificed on 7 day after injection. Initial prediction and final solution after optimization of transfer rates	48
Figure 28: Case C80F sacrificed on 1,100 day after injection. Initial prediction and final solution after optimization of transfer rates	49

List of Tables

Table 1: The characteristics of the various isotopes of Plutonium	4
Table 2: Transfer rates for the ICRP 78 systemic model for plutonium	8
Table 3: Wound Model Transfer Rates of initially soluble strongly – retained radionuclides	12
Table 4: Summary of the intramuscular injection data for non-human primates	27
Table 5: Summary of plutonium activity in Liver and Skeleton calculated using SAAM II and compared with the measured values at the time of autopsy	43
Table 6: Summary for the modified transfer rates for each case	50
Table 7: Geometric mean and GSD values with default parameters published in ICRP 78 & NCRP 156	52
Table 8: Total objective function values and corresponding AICs	53
Table 9: Exponential function values	54
Table 10: Likelihood of each model based on exponential function	55

Abstract

Eleven intravenously injected monkeys with known amounts of $^{238}\text{Pu}(\text{IV})$ citrate were analyzed using SAAM II software. The study was conducted to evaluate and optimize parameters of the ICRP 78 systemic and NCRP 156 wound model.

Retention of Pu in urine and feces from these animals has been collected on a periodic basis from the day of injection to their death. Small quantities of blood were also taken from the animals at regular intervals. After animals sacrifice, samples of bone and liver were collected. Substantial information on the translocation of radioactive materials was obtained by measuring the activities in various organs at the time of death.

The ICRP 78 systemic model and NCRP 156 wound model for plutonium were used to calculate retained activities in liver and skeleton. Retention predicted by SAAM II was compared with the known bioassay data. The predicted retention in the liver was lower for early sacrificed animals than for long lived animals after injection.

The optimization of transfer rates was attempted to improve the fits to the data by using SAAM II. Good fits for the liver and skeleton data were observed for some cases.

Chapter 1

INTRODUCTION

1.1 The Purpose of the study

A study of Pu in monkeys was begun by Durbin et al. in 1973 upon recognition that the available data at the time was insufficient for precisely describing the translocation of Pu in humans. The ^{238}Pu studies in human primates were planned to extend the small amount of data from human Pu injections, and accidental exposures in a closely related animal. The experiments were performed under controlled experimental conditions to examine the relationship between the Pu excretion rate and Pu body content and to improve the prognostic competence of the urinalysis methods used to assess occupational Pu exposure. This information was necessary to understand Pu deposition and retention in some important small organs, i.e. the endocrine glands and reproductive tract tissues (Durbin, 90).

Twenty-seven monkeys were given one intravenous or intramuscular injection with known amounts of $^{238}\text{Pu(IV)}$ citrate. Urine, feces and blood samples were taken for radioanalysis on a periodical basis from the day of injection to the death of the animal. Animals were killed from 2 hours to 1,100 days after injection. Samples of bone and all soft tissues were removed, weighed and radioanalyzed. This experiment was performed in the Division of Research Medicine and Radiation Biophysics at Lawrence Berkley National Laboratory (Durbin, 90).

The main purpose of this study is to examine the validity of the NCRP 156 default wound model coupled to the ICRP 67 default systemic model for plutonium-238 based on intravenously injected non-human primate data. This study uses ^{238}Pu activities in urine, excreta, skeleton and

liver to examine the efficacy of the NCRP 156 wound model coupled to the ICRP 67 plutonium systemic model.

The objectives are:

- Predict plutonium activity in urine and feces using the NCRP 156 wound model coupled to the ICRP 67 plutonium systemic model and compare these predictions to measured plutonium concentrations from Durbin *et. al.* data set.
- Compare predicted Pu-238 activity in liver and skeleton at time of death and the true measured activity at the time of death.
- Optimization of transfer rates for the NCRP 156 wound model coupled to the ICRP 67 plutonium systemic model for plutonium using SAAM II software in an attempt to improve biokinetic predictions of Pu-238.

Chapter 2

LITERATURE REVIEW

2.1 Plutonium

Exposures to plutonium have been the subject of significant public concern and scientific investigations for many decades. Plutonium-238 (^{238}Pu) has been used widely in thermoelectric generators and some other types of power and heat sources, but more important is that it can represent a substantial amount of the activity in spent nuclear fuel (Suslova et al. 2012).

Plutonium ($z=94$) is a silvery-gray metal that turns yellowish when exposed to air. It is primarily considered a man-made element even though scientists have found some naturally occurring Plutonium produced in some unusual geological conditions (epa.gov). The most common radioisotopes of Plutonium are Plutonium-238 with a half-life of 87.7 years, Plutonium-239 with a 2.4×10^4 years half life, and Plutonium-240 with a 6.5×10^3 years half life (ieer.org). Table 1 demonstrates some of the characteristics of the various isotopes of Plutonium.

	Pu-238	Pu-239	Pu-240	Pu-241	Pu-242
Half-life (in years)	87.74	24,110	6537	14.4	376,000
Specific activity (curies/gram)	17.3	0.063	0.23	104	0.004
Principal decay mode	alpha	alpha	alpha	beta	alpha
Decay energy (MeV)	5.593	5.244	5.255	0.021	4.983
Radiological hazards	alpha, weak gamma	alpha, weak gamma	alpha, weak gamma	beta, weak gamma	alpha, weak gamma

Table 1: The characteristics of the various isotopes of Plutonium (ieer.org)

Plutonium-238 is an energetic alpha emitter. The primary decay mode is alpha decay with decay energy of 5.593 MeV to produce the progeny Uranium-234. Plutonium-238 is primarily produced in nuclear reactors from Neptunium-237. It is used as the main power source for driving satellites and other space applications. It is the main heat source for radioisotope thermoelectric generators (RTGs) (www.ieer.org).

External exposure to Plutonium does not poses too great of a risk since it is mainly an alpha emitter. However, internal exposure can be extremely dangerous since it can stay in the body for decades, exposing various body parts to radiation and consequently increasing the risk of cancer. It is also known to cause significant effects on the kidneys (www.epa.gov).

Plutonium can enter the human body at least in two ways – inhalation and ingestion. Ingestion is considered less dangerous since a very little amount is absorbed by the stomach while the rest passes out through the digestive system. Whereas plutonium if inhaled may remain in the lungs for decades or alternately is transported to other parts of the body through the bloodstream (epa.gov).

2.2 Biokinetics of Plutonium

2.2.1 ICRP 78 Systemic Model for Plutonium

The biokinetic model for plutonium was first described in ICRP publication 67 and also later described in ICRP publication 78 (ICRP 78, 1997). The model described in ICRP 67 and ICRP 78 was modification of the model used in ICRP publication 56. The biokinetic model for plutonium is presented in Figure 1. This model is also applicable for americium, neptunium and thorium (ICRP 78, 1997).

The ICRP 78 model has several important features. The skeleton is separated into cortical and trabecular sections. Each section has three components: bone surface, bone volume, and bone marrow. The activity entering the skeleton is distributed to bone surfaces and then transferred to bone marrow by bone absorption. The activity is deduced from the transfer from bone marrow back into the blood over extended periods of time (ICRP 78, 1997).

Blood is considered to be a medium in which radionuclides are uniformly distributed. The massive soft tissues of the body are divided into three compartments: ST0, ST1, and ST2. Compartment ST0 includes the extracellular fluids and exchanges material with blood in hours or days. ST1 and ST2 compartments are intermediate-term retention which occurs over months, up

to two years and tenacious retention which needs involve mechanisms requiring years (ICRP 78, 1997).

The liver compartment is divided into two compartments: Liver 1 and Liver 2. The liver 2 compartment correspond to tenacious retention where the biological retention halftime is greater then 1 year and liver 1 that has half-life equal to 1 year. The liver is considered as a medium where radionuclides are deposited uniformly. The liver loses activity to blood and the gastrointestinal tract with half-life of 1 year (ICRP 78, 1997).

The Kidneys compartment contents of two compartments: kidney tissue and urinary path. The urinary path loses activity to urine through urinary bladder contents and kidney tissue interchanging activity with the blood (ICRP 78, 1997).

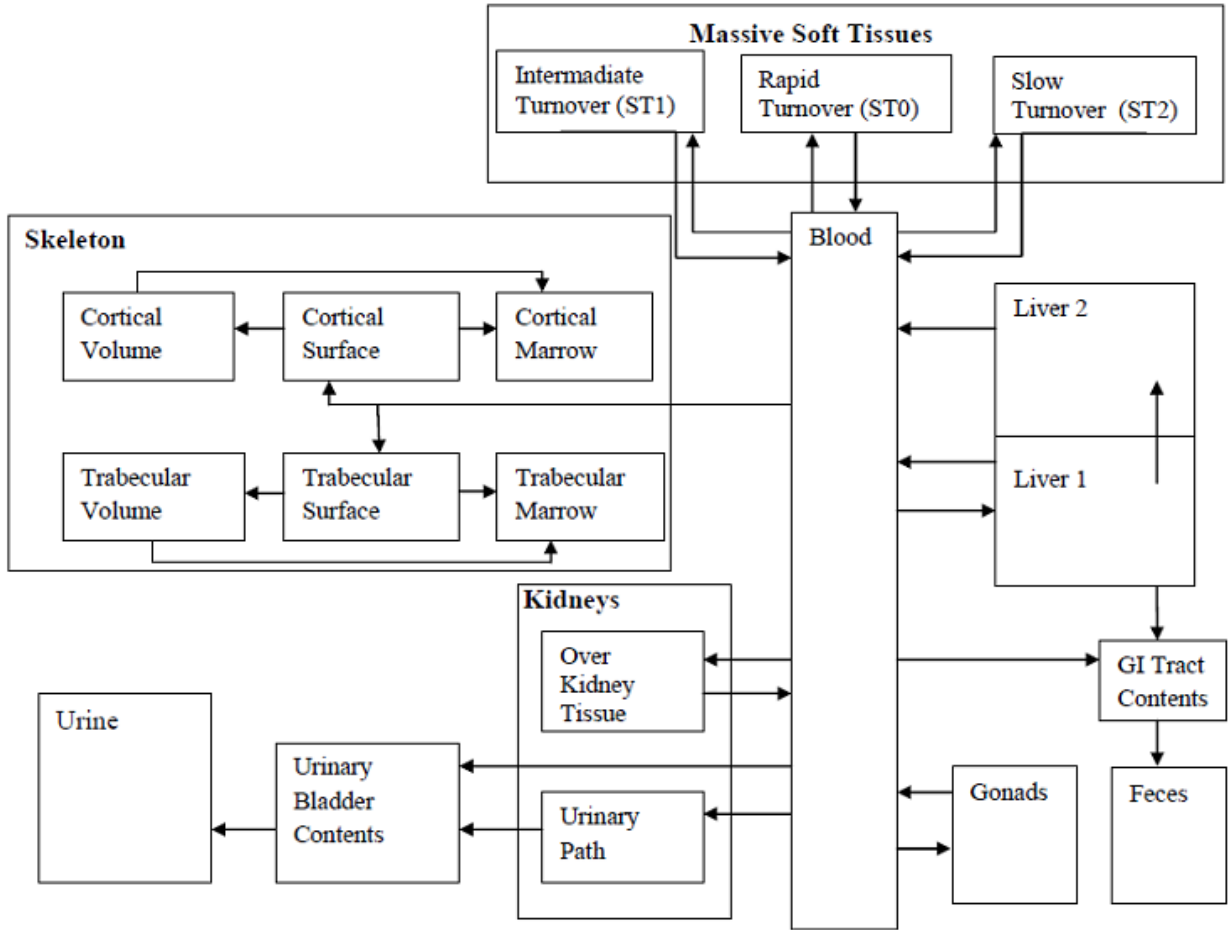


Figure 1: ICRP 78 Systemic model for Plutonium (ICRP, 1997)

Route of transfer between compartments		Transfer Rate (d ⁻¹)
From	To	Default
ST0 ^a	Blood	0.693
ST1 ^a	Blood	0.000475
ST2 ^a	Blood	0.000019
Trabecular marrow	Blood	0.0076
Cortical marrow	Blood	0.0076
Other kidney tissue	Blood	0.00139
Liver2	Blood	0.000211
Testes	Blood	0.00019
Ovaries	Blood	0.00019
Blood	ST0	0.2773
Blood	ST1	0.0806
Blood	ST2	0.0129
Blood	Trabecular surface	0.1941
Blood	Cortical surface	0.1294
Trabecular surface	Trabecular volume	0.000247
Cortical surface	Cortical volume	0.0000411
Trabecular surface	Trabecular marrow	0.000493
Trabecular volume	Trabecular marrow	0.000493
Cortical surface	Cortical marrow	0.0000821
Cortical volume	Cortical marrow	0.0000821
Blood	Other kidney tissue	0.00323
Blood	Liver1	0.1941
Liver1	Liver2	0.00177
Blood	Testes	0.00023
Blood	Ovaries	0.000071
Liver1	Small intestine	0.000133
Blood	Upper large intestine	0.0129
Blood	Urinary path	0.00647
Blood	Bladder	0.0129
ST1	Bladder	0.000475
Urinary path	Bladder	0.01386
SI ^b	ULI	6
ULI ^c	LLI	1.8
LLI	Feces	1
Bladder	Urine	12

Table 2: Transfer rates for the ICRP 78 systemic model for plutonium (ICRP 78, 1997)

^aST – soft tissue

^bS.I. – small intestine

^cU.L.I. – upper large intestine

2.2.2 NCRP 156 Wound Model for Plutonium

NCRP Report 156 provides a review of scientific data to explain the behavior, deposition and retention of radioactive materials at the wound site, and clearance of radionuclides injected intramuscularly (i.m.) or subcutaneously (s.c.) in animals. The NCRP wound biokinetic model consists of seven compartments, where five of them are considered to be relatively tissue insensitive and independent of the wound location. These five compartments are reflecting the biochemical and physiochemical properties of the foreign substance that has entered the body by the wound. Those are fragment, soluble, colloid & intermediate state (CIS), particle aggregates & bound state (PABS), and trapped particles & aggregates (TPA). The two last compartments of the wound model are blood and lymph nodes. The general wound model is shown in Figure 2 (NCRP, 2007).

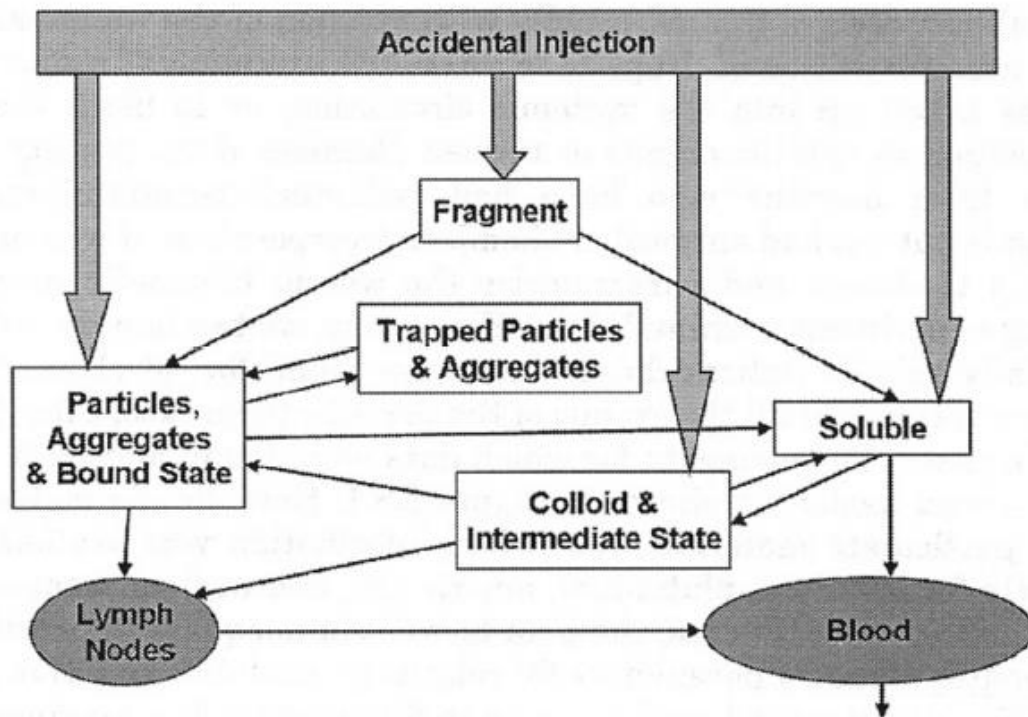


Figure 2: NCRP general wound model (NCRP, 2007)

In this model, radionuclides are initially introduced into the wound site considered to be in solution, or as colloidal, particulate or fragments in suspension. The Report 156 considers fragments and particles as solids. In this Report, Plutonium-238 is categorized as soluble (NCRP, 2007).

Radionuclides were categorized according to the fraction of the injected activity remaining after an i.m. injection at the wound site from 1 to 64 days past injection, and expressed as percent of injected dosage (% ID). Equation 1, provided in NCRP 156 describes retention of soluble radionuclides after an intramuscular injection at the wound site:

$$R(t) = \sum_i A_i e^{-\lambda_i t} \quad \text{Equation 1}$$

Where

$R(t)$ = radionuclide retention at the wound site (% ID)

A_i = the partition coefficient

λ_i = the retention rate constant for retention component i

t = days after deposition

The solubility of foreign materials, which predicts their retention, is classified into four categories: weakly – retained, moderately – retained, strongly – retained, and avidly – retained radionuclides. Plutonium–238 is classified as a strongly retained radionuclide. Wound retention for this category was 32 to 85% at 1 d, and following slow clearance reduced retention to 8 to 40% at 64 days post injection. The compartment wound model for plutonium-238 is presented in Figure 3 (NCRP, 2007).

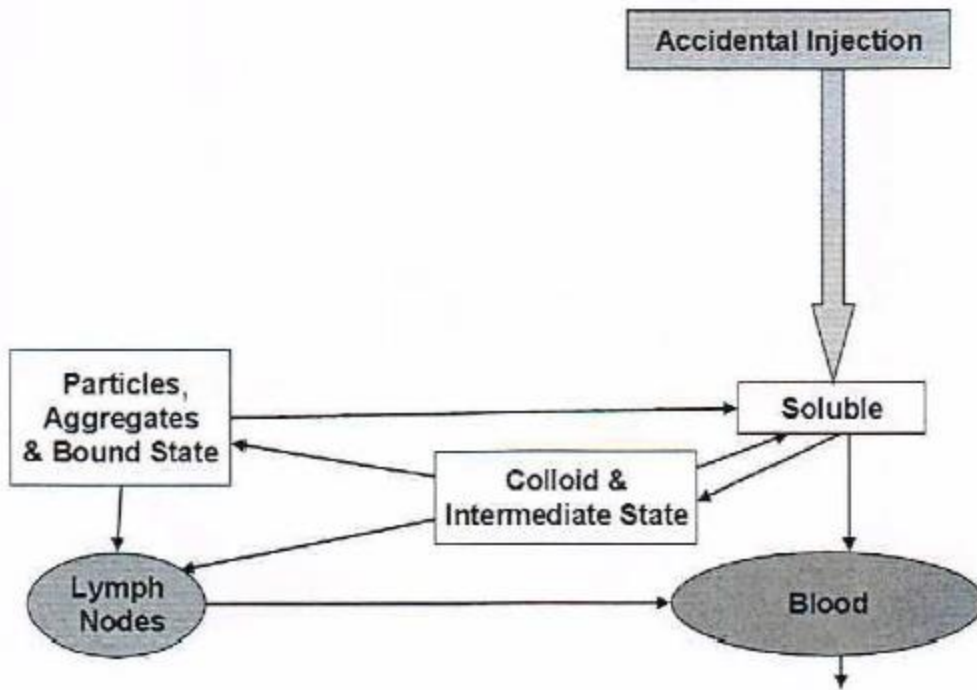


Figure 3: Wound Model for Injection of Soluble Substances (NCRP, 2007)

The transfer rates for wound site retention for each pathway are presented in Table 3. Equation 2 describes wound retention of strongly retained radionuclides:

$$R(t)_{strong} = 50e^{-1.1t} + 32e^{-0.029t} + 18e^{-0.00086t} \quad \text{Equation 2}$$

Where

$R(t)_{strong}$ = the retention a in a deep puncture wound (% ID)

t = the days after deposition

Pathway	Transfer Rate (d⁻¹)
Soluble to Blood	0.67
Soluble to CIS	0.60
CIS to Soluble	0.024
CIS to PABS	0.0097
PABS to Soluble	0.0012
PABS to Lymph nodes	0.00002
Lymph nodes to Blood	0.029

Table 3: Wound Model Transfer Rates of initially soluble strongly – retained radionuclides
(NCRP, 2007)

2.3 Retention and Translocation of Systemic Pu

Since the nearly four decades since Pu-injected humans were first studied, there have been numerous investigations of the behavior of Pu in laboratory animals, in accidentally exposed workers, and in populations exposed only to the small activities in fallout. Several models of the metabolism of Pu in humans have now been developed (Leggett, 1985). Between 1945 and 1946, eighteen fatally ill humans were injected with tracer concentrations of plutonium citrate or nitrate to establish the relationship between urinary excretion and body content of Pu in humans (Leggett, 1985). Measurements of activity in excretion of these subjects were made regularly during the first few weeks after injection, and a few supplementary measurements were made with two of the subjects through 1,645 d post injection.

A model was developed to explain retention, translocation, and excretion of Pu found in the blood stream of an adult human. A diagram of the model and the direction of movement of activity among compartments are given in Figure 4. Figure 4 shows those parameters describing the distribution of Pu among organs as well as those describing retention in the skeleton. These parameters depend on age even during maturity (Leggett, 1985).

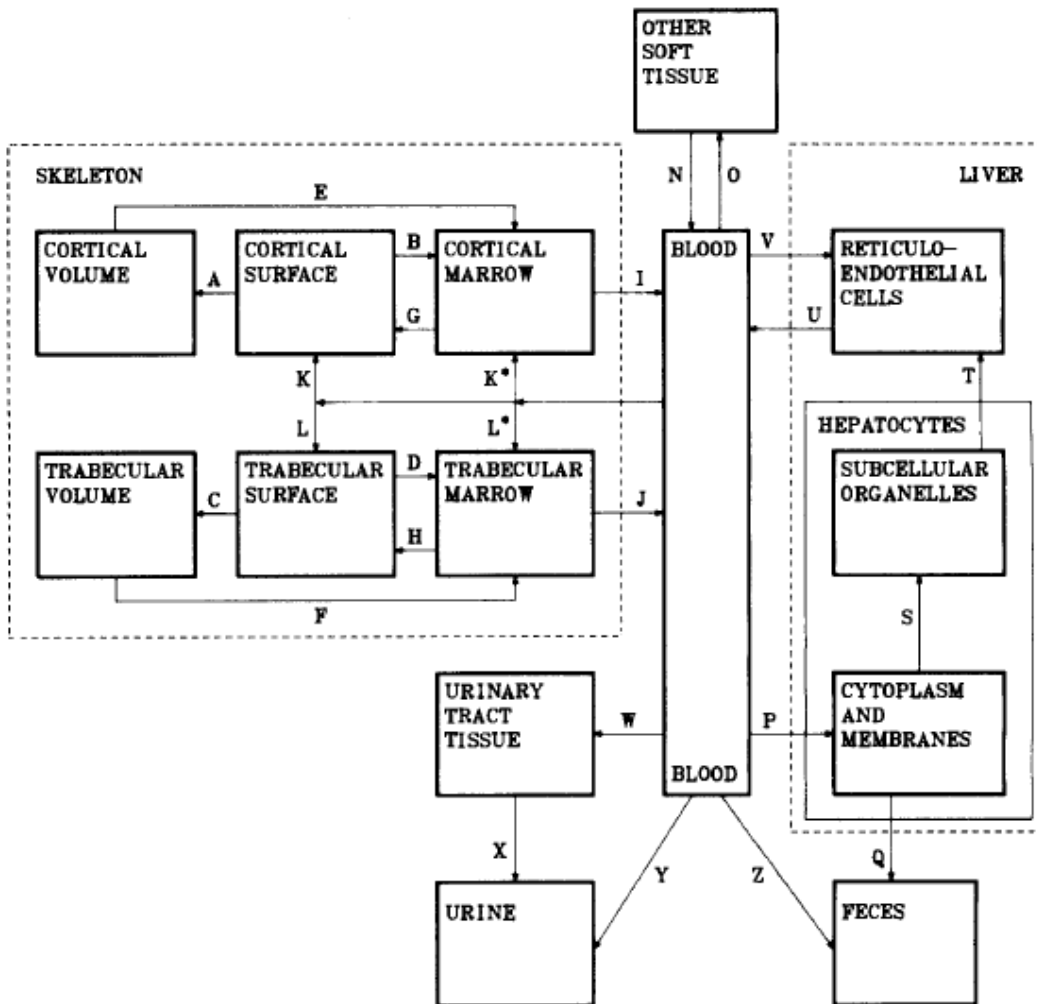


Figure 4: Diagram of the compartments used in the model and the direction of movement of Pu among these compartments (Leggett, 1985).

2.3.1 Deletion from the blood

It is possible that Pu could be present in blood in a wide distribution of solubility classes. For convenience only two relative solubility classes will be distinguished here: soluble (that entering blood in ionic or monomeric form) and insoluble (that entering the blood as insoluble particles, colloids, or polymers). Soluble Pu that has reached the blood stream may become entrapped in some of the body's Fe transport and storage systems. Much of the Pu(IV) in blood

serum complexes with transferrin, the Fe-transport protein, and a substantial fraction of systemic Pu appears to be carried by transferrin to bone marrow and to liver (Leggett, 1985).

Plutonium circulating in the blood after administration of relatively soluble forms may also bind to citrate, and it may be mainly the citrate complex that is excreted in urine. It is also possible that some unbound Pu may be filtered by the kidney and excreted in urine (Leggett, 1985).

2.3.2 Distribution and retention in the skeleton

Due to the heterogeneous nature of Pu distribution on bone surfaces and its different rates of removal from various parts of the skeleton, it is convenient to view the skeleton as divided into two principal parts: cortical (or compact) bone and trabecular (or spongy or cancellous) bone. These two bone types are usually defined by their surface to volume ratios, which are much larger for trabecular bone. Both bone types are found in all bones, but the comparative amounts of each vary significantly from one bone to another. Much of the cortical bone in the body is found in the shafts of the long bones, where it surrounds the marrow cavities. Trabecular bone is composed as a network of fine interlacing partitions (trabeculae) enclosing cavities containing red or fatty marrow. Trabecular bone is found mostly in the vertebrae, in the flat bones, and in the ends of the long bones. Cortical bone contains about 80% of the adult mineralized skeleton and trabecular bone about 20%, by volume, by mass, and by mineral content. Both bone types are continuously undergoing remodeling, which involves the removal and replacement of bone mineral. As a base case value it is assumed that 80% of soluble Pu entering blood is separated between the skeleton and liver independent of age; this relates to the initial exposure as well as to recycled activity (Leggett, 1985).

2.3.3 Distribution and translocation in the liver

Beagle and rat investigations have led to the following model imply the following scheme for hepatic uptake and the translocation of Pu reaching the blood stream in soluble form. The element is first attached to transferrin and transported to the liver, where it may be released at the membranes of the hepatocytes. Inside the hepatocytes, Pu is connected at first with the Fe-storage protein, ferritin. It has been shown that Pu (IV) could transfer to ferritin *in vitro* at physiological pH and that the Pu⁻ ferritin complex is more stable than the Pu⁻ transferrin complex. Within a few weeks, Pu leaves the cytoplasm and becomes connected with subcellular structures, principally lysosomes, microsomes, and mitochondria. After a few months, the hepatic cells die and their debris, including Pu, is taken up by the reticulo-endothelial. In the dog liver, Pu in RE cells is associated with hemosiderin, and Fe-storage compounds (Leggett, 1985).

It is assumed that one-third of the Pu in feces is from liver bile and that the daily clearance of Pu in feces represents about 0.024 times the activity in blood at times remote from injection (Leggett, 1985).

2.3.4 Soft Tissues

Soluble Pu may be carried by transferrin to the different organs and probably released at the same locations as Fe. Whereas insoluble forms of Pu will be taken up by RE cells in soft tissues as well as in the liver and bone marrow. It is obvious from data from Pu-injected humans that a substantial portion of Pu is lost from soft tissues throughout the first few months after injection. Because a small quantity of Pu is excreted for this period of this time, it becomes evident that activity lost from other soft tissues is taken up by the skeleton and liver. The activity removed from blood and not entering the non-biliary excretion pathways, that is, not going

directly to feces or urine, and not entering the tissues of the urinary tract and which represents about 20% of the intake is assigned to other soft tissue (Leggett, 1985).

2.3.5 Excretion

It becomes an implicit aspect of Pu translocation that Pu enters the urine directly from blood via the kidney or indirectly from blood after a temporary residence in the kidneys, bladder, or urethra. Entrance into feces is assumed to be either in liver bile or in other digestive secretions or desquamated intestinal cells. There may be small quantities of urinary excretion at early times post Pu intake that enters the blood stream in aggregate form. No more than 0.04% of Pu injected into beagles in polymeric form was excreted in urine at 14 d after injection (Leggett, 1985).

Chapter 3

Materials and Methods

3.1 SAAM II

The Simulation, Analysis and Modeling (SAAM) software version II allows one to build the model using a compartmental or numerical application. In SAAM II, compartmental applications allow the user to choose from a set of model-building tools representing compartments, transfers, and delays to build a graphical representation of a compartmental model on a drawing canvas (Fig. 5). The user then defines attributes for each object in the model using dialog boxes. The compartmental application is described by the system of differential equations. The name of the transfer coefficients are shown on Figure 6:

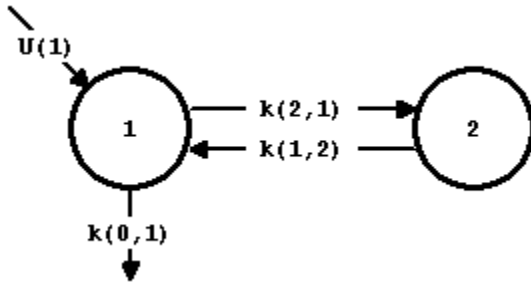


Figure 5: Name of the transfer coefficients

The SAAM II pattern for the transfer coefficients $k(i, j)$ is $k(to, from)$, where $k(2,1)$ is the transfer rate compartment 2 from compartment 1. Every object on the drawing canvas has a related dialog box, where reference names, input type and initial amount can be entered.

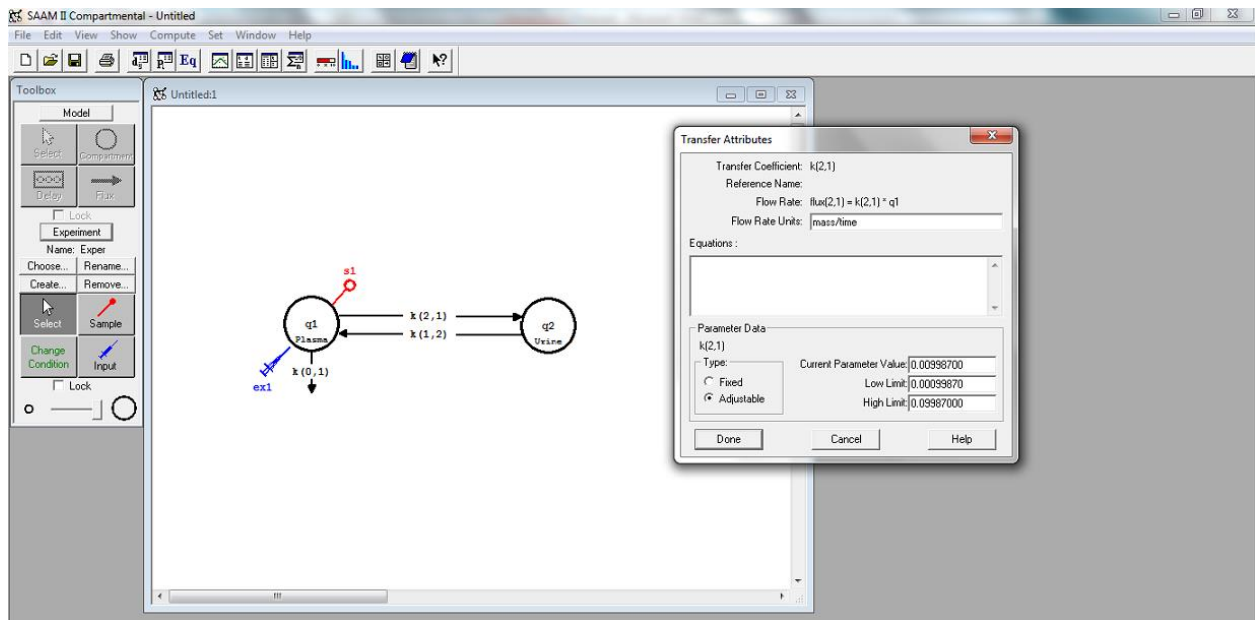


Figure 6: SAAM II main window with four main areas: the menu bar, the toolbar, the toolbox, and the drawing canvas

3.2 Methods of Analysis

The software package for Simulation, Analysis and Modeling (SAAM) version II was used in this study. The SAAM II package was developed for kinetic analysis of experiments in pharmacokinetic studies. Using the SAAM II compartmental model and its model building tools the graphical representation of the ICRP 78 Pu systemic model coupled to NCRP 156 wound model was created. The parameter values were allocated to each transfer path based upon ICRP 78 as coupled to NCRP 156 employing default transfer rates (Figure 7). Using a dialog box, the elements for each compartment were defined and a system of differential equations was created automatically to represent the model used.

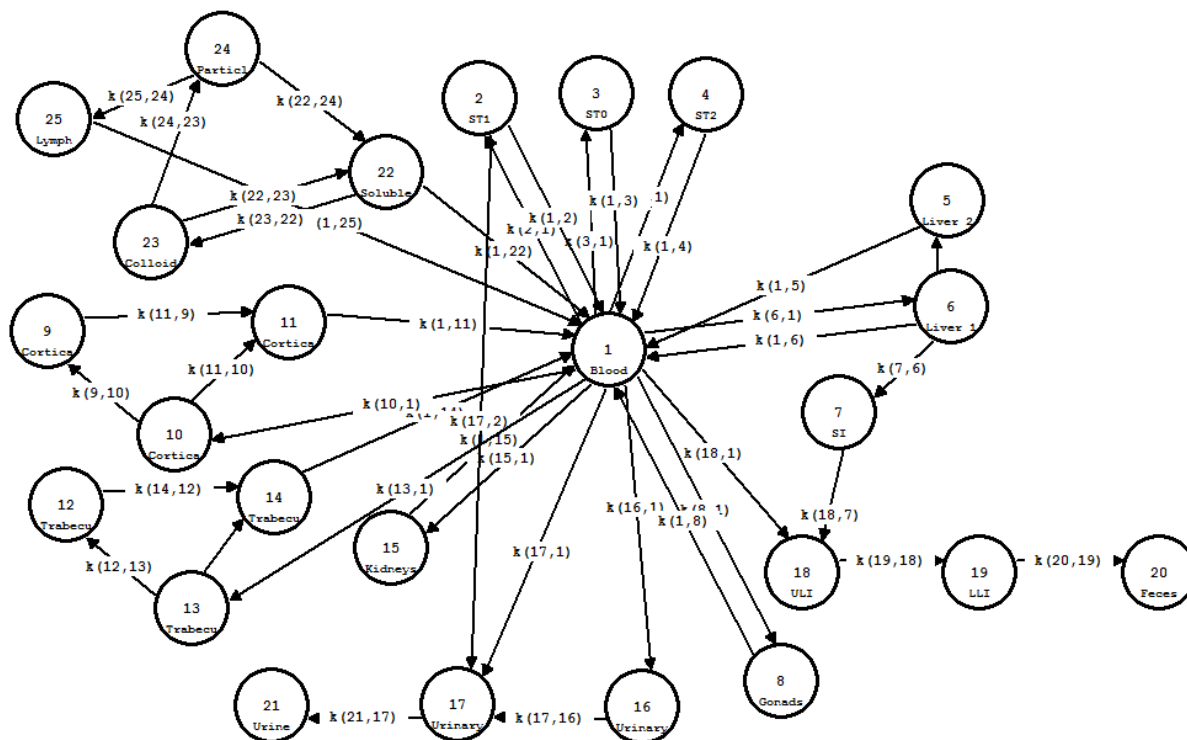


Figure 7: Schematic illustration of the ICRP 78 systemic model coupled to NCRP 156 wound model for plutonium in SAAM II

An experiment was performed on a model by choosing from a set of experiment-building tools which were characterized as inputs and outputs. SAAM II automatically included inputs to the differential equations so that there was a connection of experimental measurements incorporated in a data table. Once the model was specified, SAAM II fitted the model to the data. SAAM II adjusted the values of the model parameters to obtain the best fit between the calculated values and the data. The output was presented in graphical form.

Considering this case in which the wound model was coupled to the ICRP 78 systemic model, plutonium was mathematically injected into soluble compartment (#22). The initial amount of injection was a normalized value intended to be equivalent to 100% of the initial activity, as it shown in Figure 8.

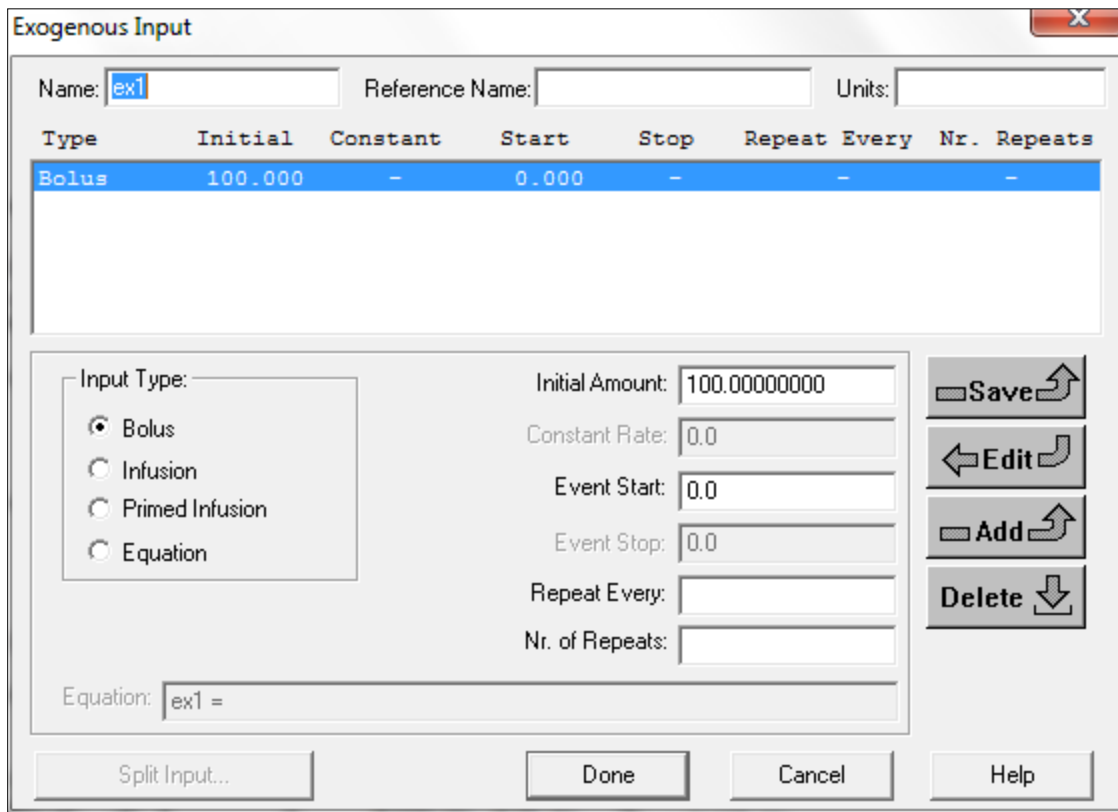


Figure 8: Input Window for Initial Amount of Activity in SAAM II

The Bayesian option was chosen as the modification type. The transfer rates were optimized between lower and higher limits. Lower and higher limits were chosen arbitrarily to be 1/10 and 10 times the transfer rate, respectively. The population mean and standard deviation are calculated if the Bayesian option is selected, as shown in Figure 10.

The data window was used to enter the bioassay measurement data for urine, feces, liver, and skeleton deposition. An example of the data window is shown in Figure 10.

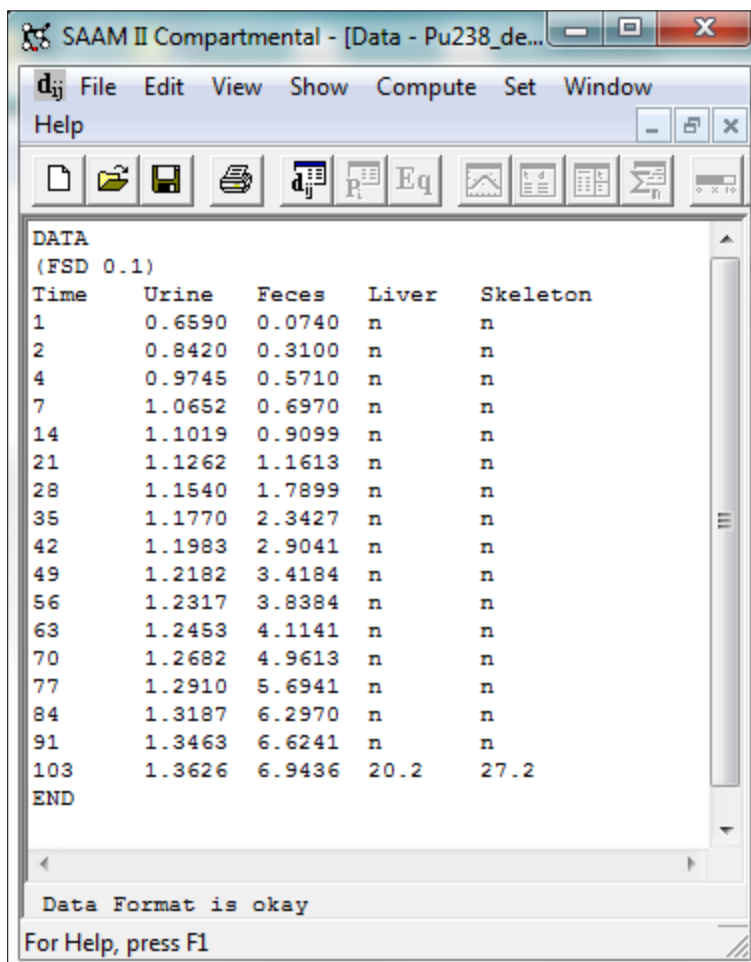


Figure 9: The data window in SAAM II

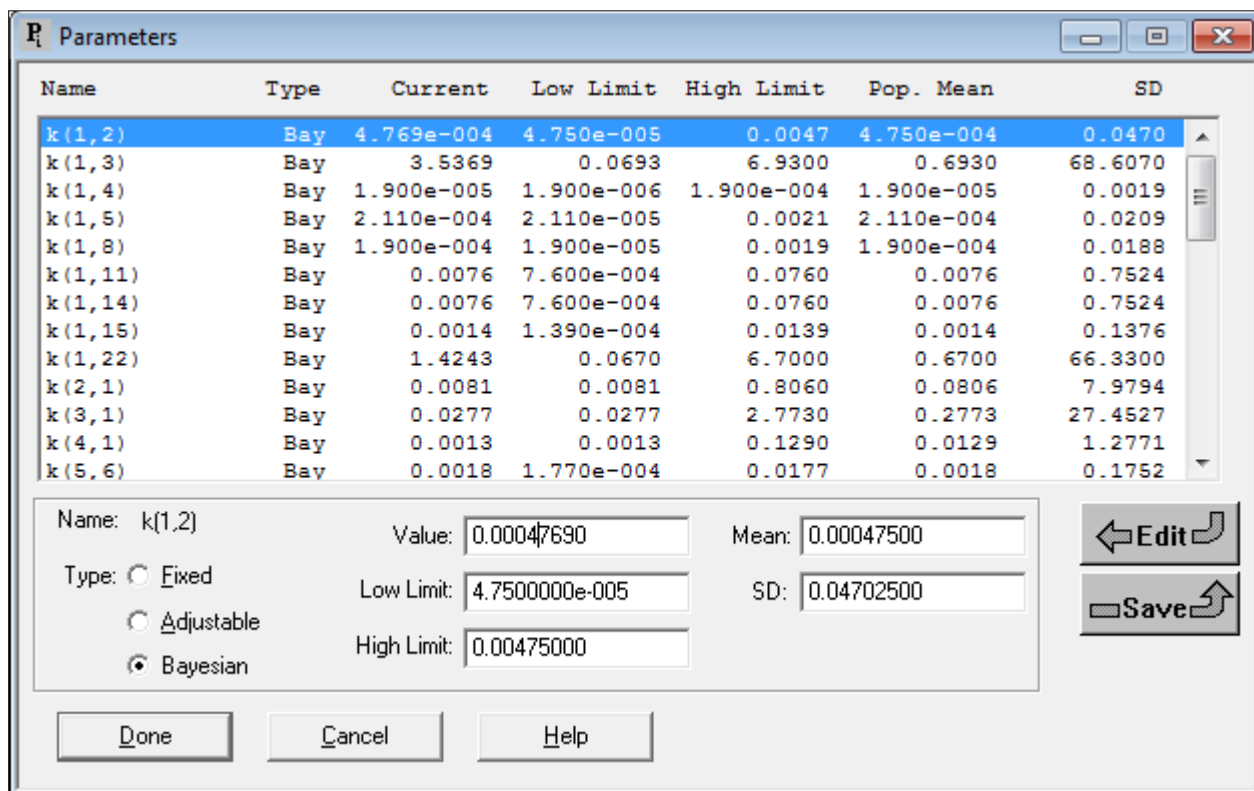


Figure 10: Parameter window in SAAM II

SAAM II fits the model to the bioassay measurement data by optimizing the values of the transfer rates among model compartments. SAAM II stops the optimization process after it obtains the iteration limit. As a product of the optimization process, three fit-parameters are calculated: total objective function, the Akaike information criterion (AIC) and the Schwarz-Bayesian information criterion (BIC). The importance of these fit parameters is described below.

3.3 Total Objective Function

The total objective function provides a calculation of the prediction error between the values predicted by the model and the observed values. This difference is frequently referred to as the residual in many statistical fitting routines. The objective of the SAAM II optimization is to

minimize the residuals. The model function is minimized to best fit the model to the data. The primary reason of fitting the data is to find a potential model based on the observed values. A Bayesian estimation technique is employed within SAAM II as an algorithm for parameter estimation. The Bayesian estimation for a parameter p_k is given by the following equation:

$$R(p) = \frac{1}{M} \left\{ \sum_{j=1}^J \sum_{i=1}^{N_j} \left(\log[v_{i,j}(s(\hat{p}, t_{i,j}), v_{i,j}, \hat{v}_j)] + \frac{(y_{i,j} - s(\hat{p}, t_{i,j}))^2}{v_{i,j}(s(\hat{p}, t_{i,j}), y_{i,j}, v_{i,j})} \right) + \sum_{k=1}^{N_b} \frac{(p_k - m_{p,k})^2}{\sigma_{p,k}^2} + \log(\sigma_{p,k}^2) \right\} \quad \text{Equation 3}$$

Where:

$R(p)$ = objective function

p = vector of adjustable parameters

$y_{i,j}$ = i^{th} datum in the j^{th} data set

$s(\hat{p}, t_{i,j})$ = model value corresponding to the $y_{i,j}$ at the time $t_{i,j}$

v_j = variance parameter in the j^{th} data set

$v_{i,j}(s(\hat{p}, t_{i,j}), y_{i,j}, v_{i,j})$ = variance model for $y_{i,j}$

M = total number of data points

J = number of data sets

N_j = number of data points in the data set

$m_{p,k}$ = mean value of p_k (population mean)

$\sigma_{p,k}$ = standard deviation of p_k in that population

3.4 The Akaike Information Criterion (AIC) and the Schwarz-Bayesian Information Criterion (BIC)

SAAM II provides the values of the Akaike Information Criterion (AIC) and the Schwarz-Bayesian Information Criterion (BIC). The Akaike Information Criterion (AIC) is used to compare various statistical models. It provides information regarding the relative goodness of fit of a statistical model. Usually, the model with minimum AIC is the one that is closest to the observed data (Akaike, 1974:1978). The concept of AIC was first introduced by Hirotugu Akaike in the 1970's (Hirotugu, 1974). AIC is defined using the following equation

$$AIC = -2 \log(L) + 2K \quad \text{Equation 4}$$

Where:

L = maximized value of the likelihood function for the model

K = number of estimable parameters

Individual AIC values have no special meaning and are not unique, but the difference in AIC between any two models, ΔAIC , is meaningful. The model with the smallest AIC value is considered the best fit to the data. Although AIC is useful in terms of selecting the best model from a set of fits, it does not provide any information regarding the quality of the model. Thus, if all provided models are poor, AIC will just select the best one among them irrespective of how poor the model might be in reality. The AIC difference is defined using the following equation

$$\Delta AIC_i = AIC_i - AIC_{min} \quad \text{Equation 5}$$

Where:

ΔAIC_i = AIC difference

AIC_i = AIC value of the i^{th} model

$$AIC_{\min} = AIC \text{ of the best model}$$

In general, models with $\Delta AIC_i \leq 2$ have substantial support, models with $4 \leq \Delta AIC_i \leq 7$ have considerably less support, and models with $\Delta AIC_i > 10$ have essentially no support (Burnham and Anderson, 2002).

AIC differences can be exponentiated, producing a ratio of the relative likelihood of two models. The relative likelihood of any two models can be found by:

$$\exp\left(\pm \frac{1}{2} \Delta AIC\right) \quad \text{Equation 6}$$

Where ΔAIC is the difference in AIC values. It is usually easiest to interpret this ratio if it is computed to be greater than 1.0.

The Schwarz-Bayesian Information Criterion (BIC) is also based on the maximum likelihood function like the Akaike Information Criterion (AIC). The model with the smallest BIC is the one that is considered to have the maximum posterior probability. The BIC is defined by the following equation

$$BIC = -2 \log(L) + K \log(n) \quad \text{Equation 7}$$

Where:

L = maximized value of the likelihood function for the model

K = number of estimable parameters

n = sample size

Chapter 4

RESULTS AND DISCUSSIONS

4.1 SAAM II Prediction based on ICRP 78 Systemic Model coupled to NCRP 156 wound

Model

Injections of plutonium were made intramuscularly into eleven non-human primates. The summary of 11 non-human primates injected with $^{238}\text{Pu(IV)}$ citrate sacrificed from 2 hours to 1,100 days post injection is given in Table 4. The excretion data were analyzed from the day of injection to death. The samples of urine and feces were analyzed to determine the amount of plutonium present.

No.	Case	Injection Dosage (uCi/kg)	Weight (kg)	Age at time of injection, y	Days Between Injection and Death
1	C95F	2	4	>10.5	8 d
2	C103F	1.06	2	4.8	20 hours
3	C77F	1.17	4	>11	2 hours
4	C80F	0.31	5.22	>13	1100 d
5	C108F	1	4	>6.3	18 hours
6	C131F	0.3	4.88	8	56 d
7	S114F	0.34	11.4	>8	7 d
8	R186M	0.35	7.71	17	103 d
9	C166M	0.48	7.3	>9	106 d
10	C145M	0.36	5.79	>10	7 d
11	C106M	0.34	7.3	6.7	106 d

Table 4: Summary of the intramuscular injection data for non-human primates

All values of the predicted and measured concentration of plutonium in urine and feces were compared as a function of the time.

Figures 11 through 23 provide plots that demonstrate the difference between measured data and predicted values based on the default parameters described in the ICRP 78 systemic model coupled to the NCRP 156 wound model as fitted using the software package SAAM II.

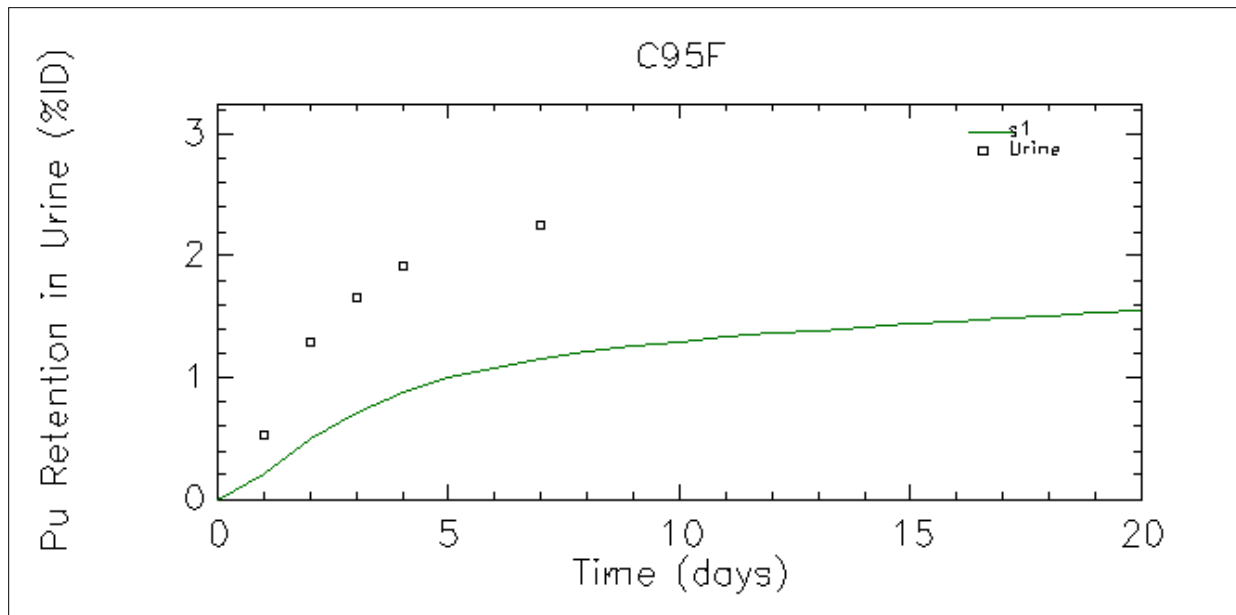
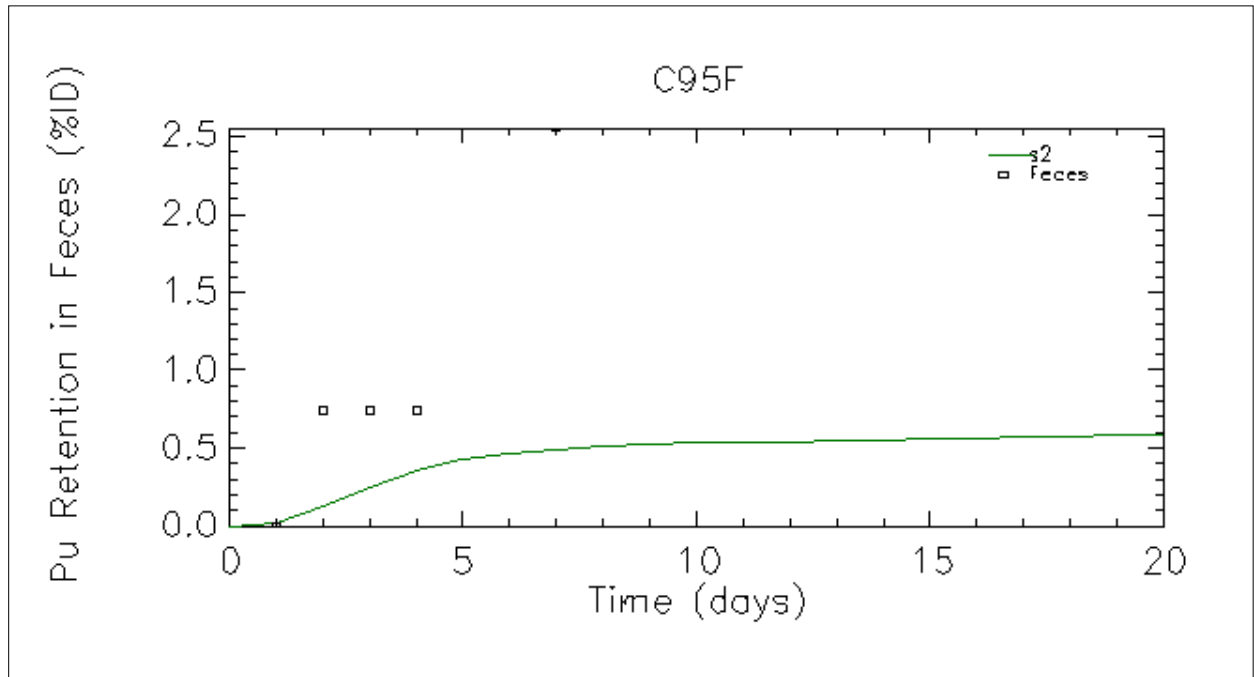


Figure 11: Case C95F sacrificed 8 days after injection

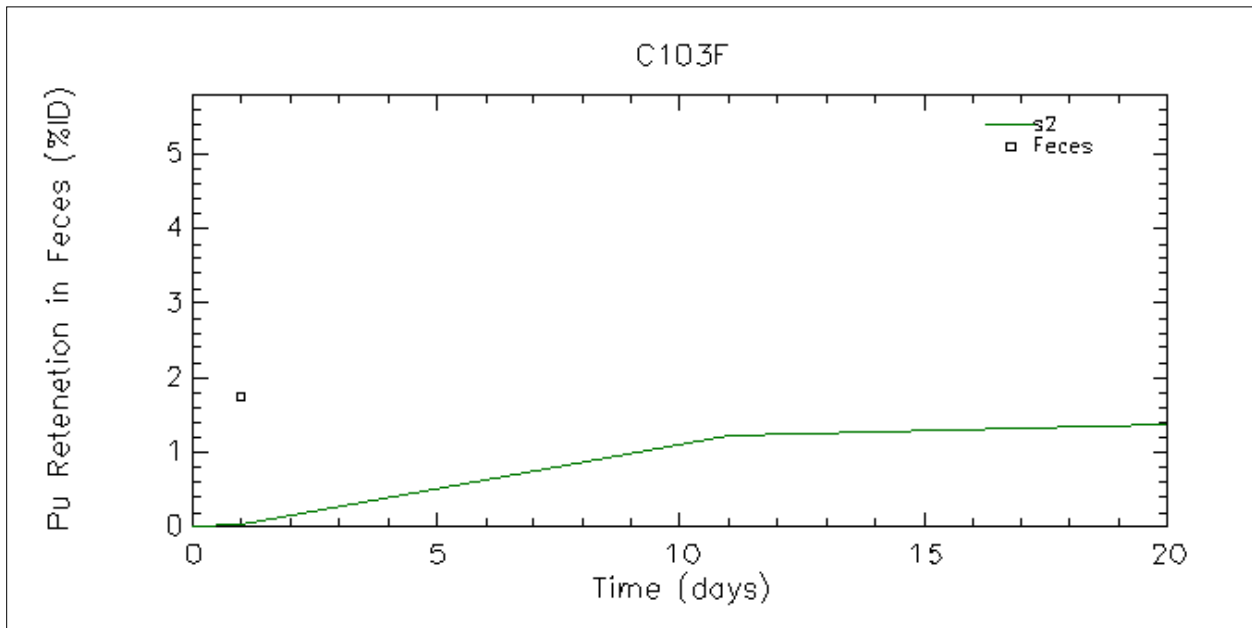
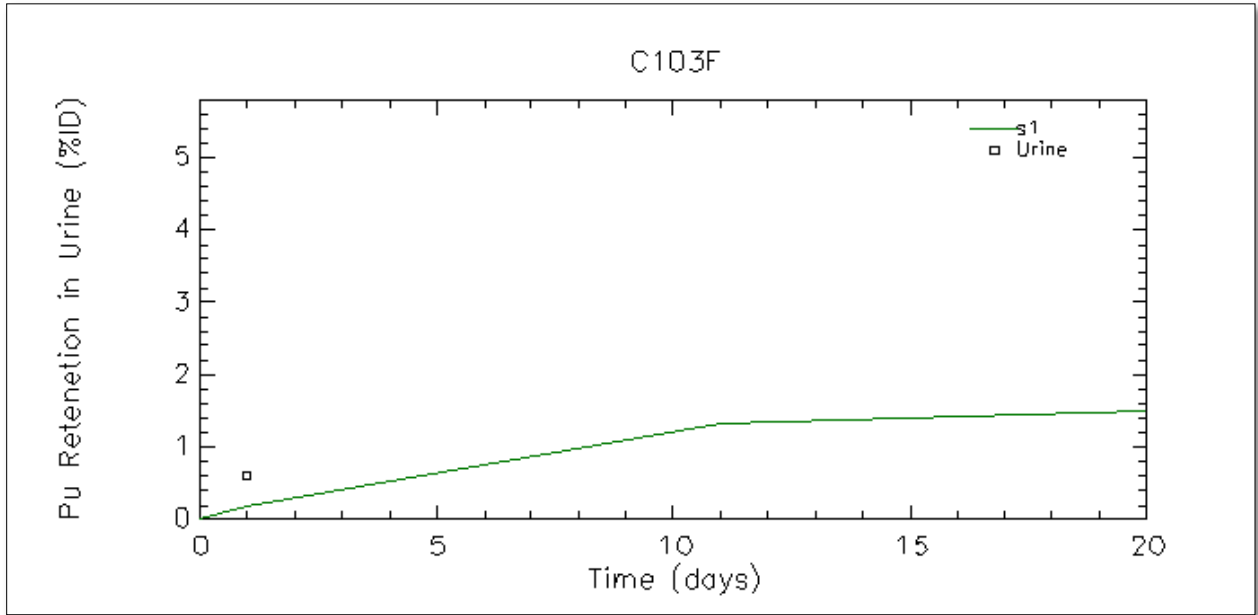


Figure 12: Case C103F sacrificed 20 hours after injection

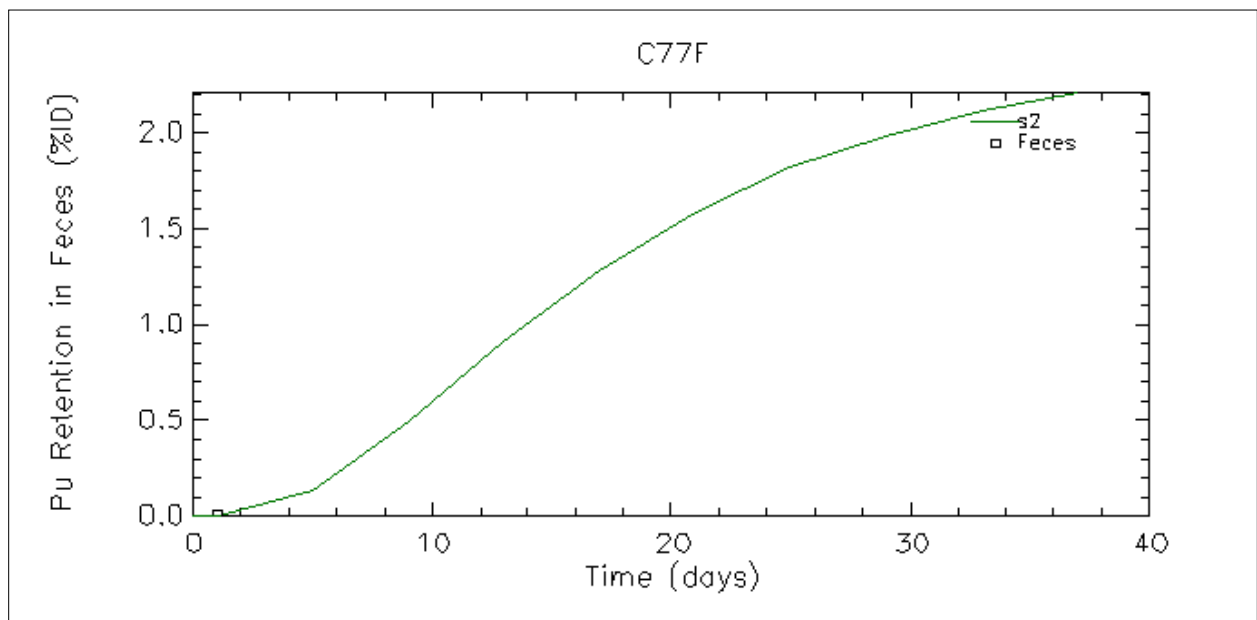
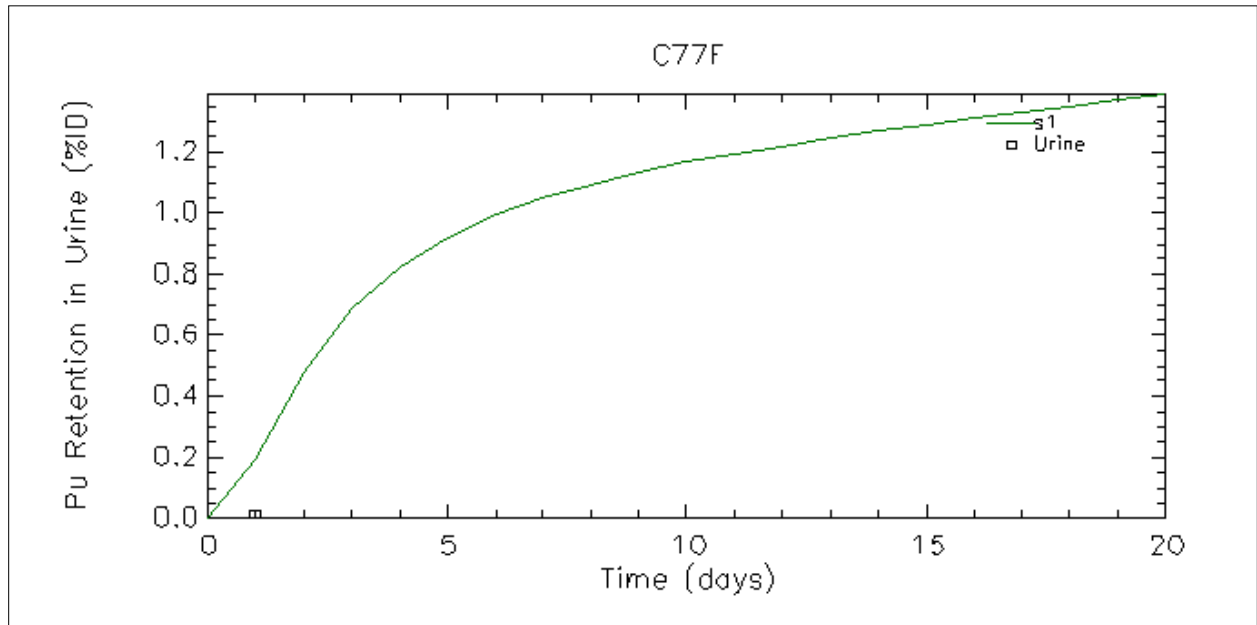


Figure 13: Case C77F sacrificed 2 hours after injection

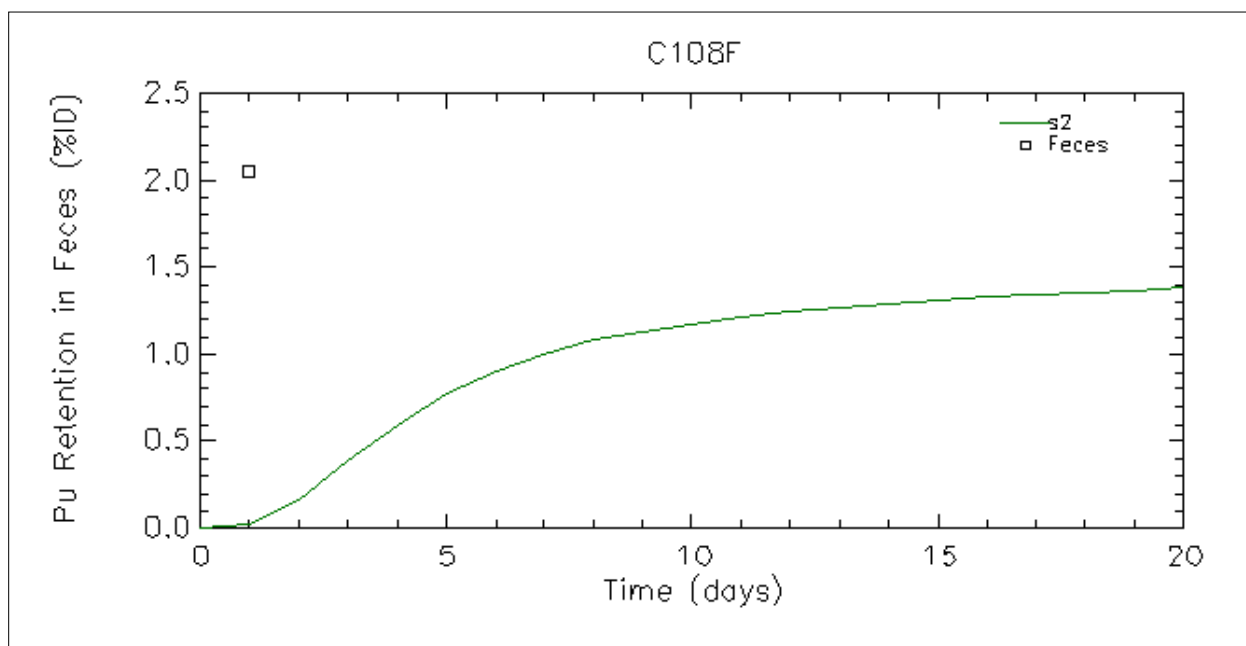
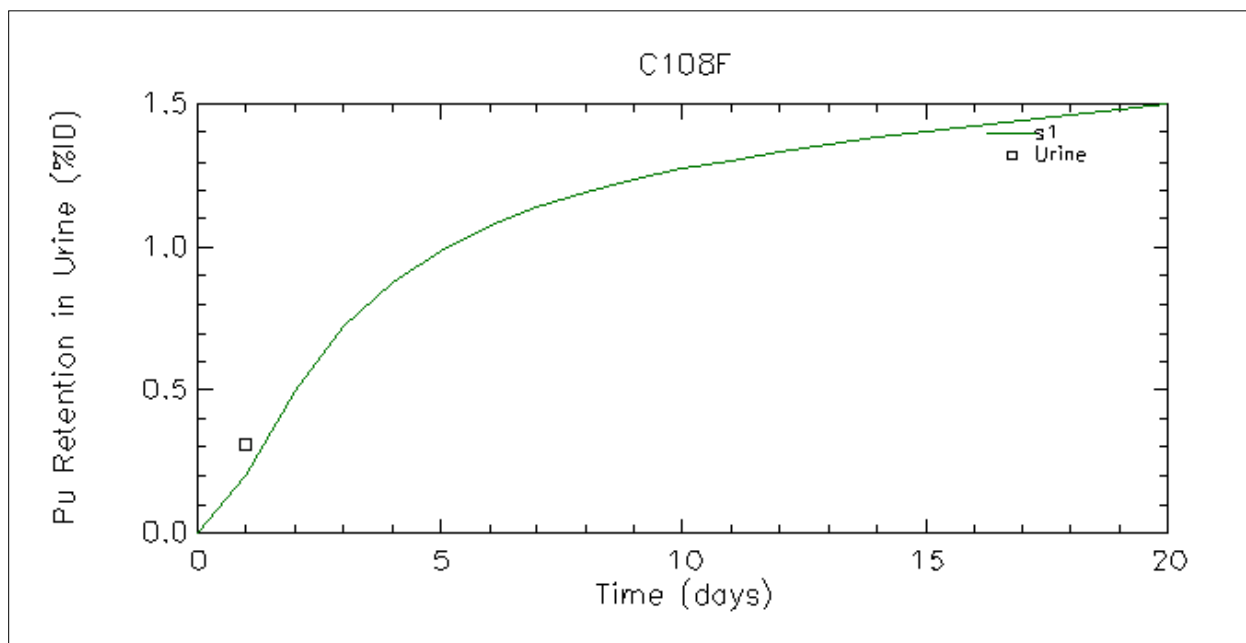


Figure 14: Case C108F sacrificed 18 hours after injection

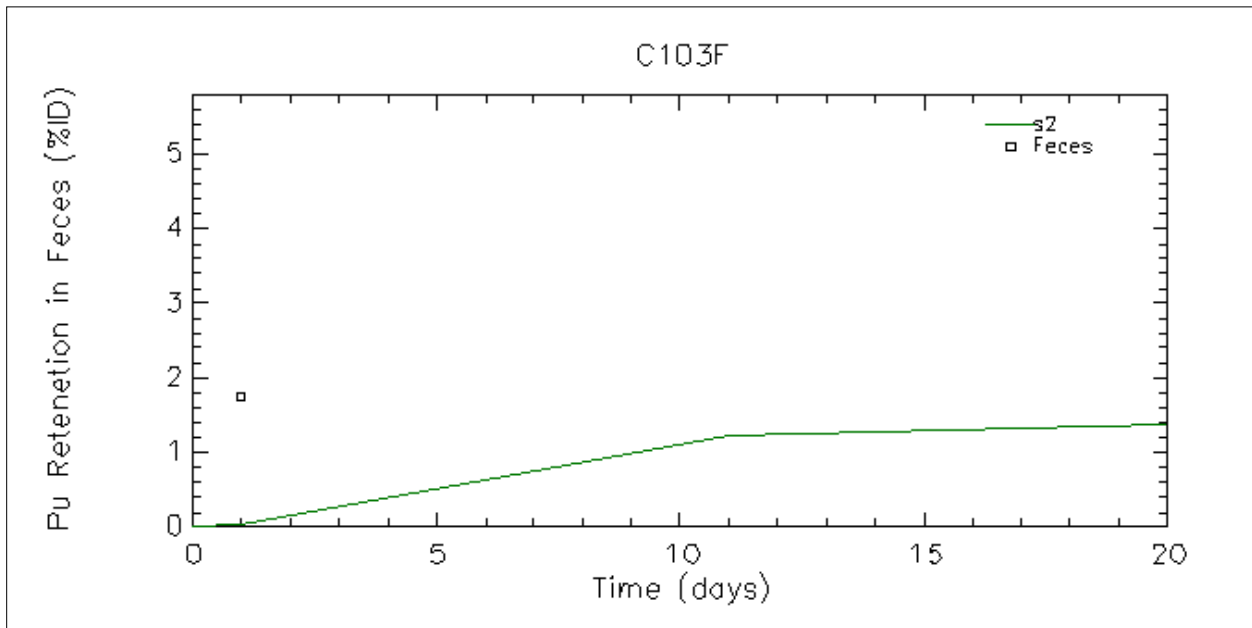
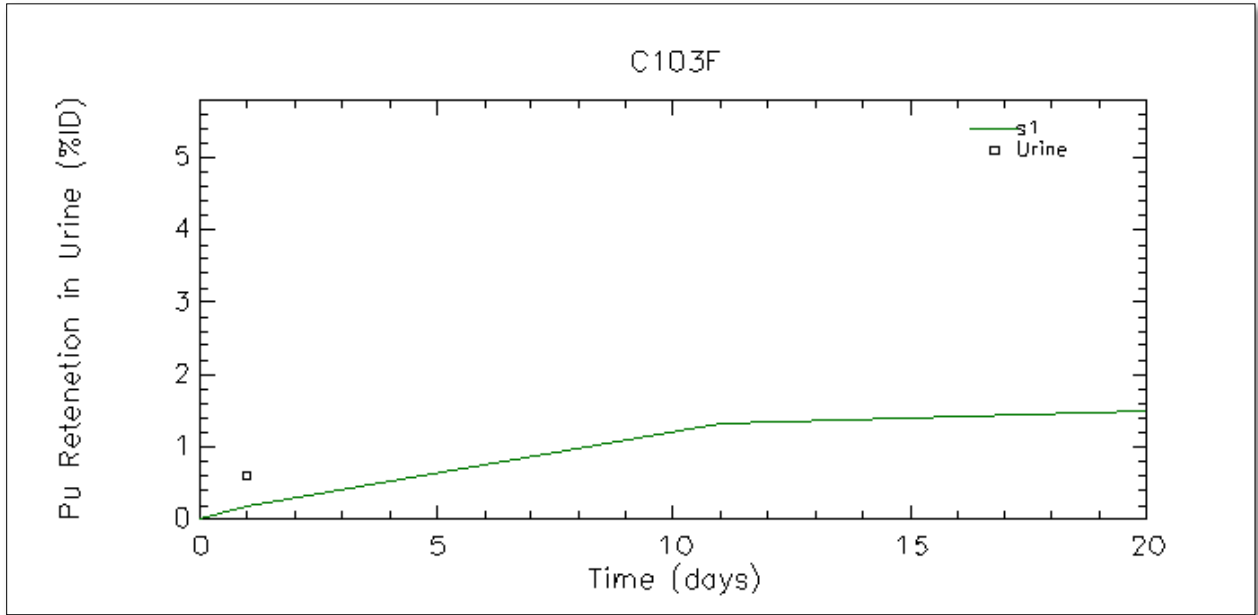


Figure 15: Case C103F sacrificed 20 hours after injection

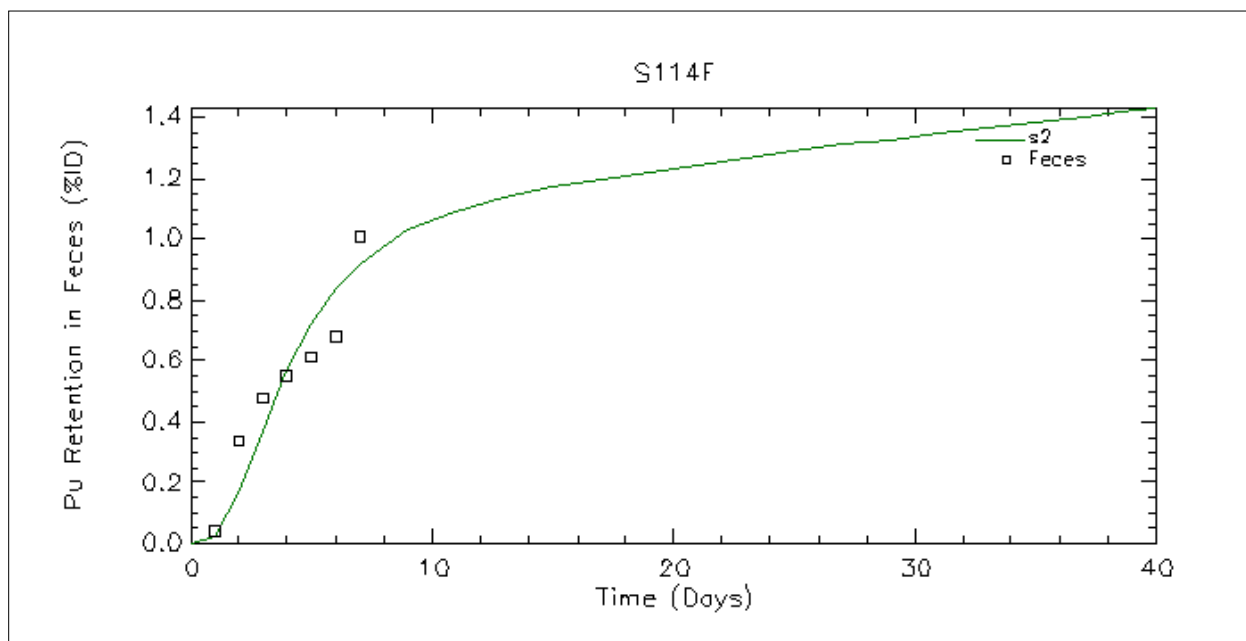
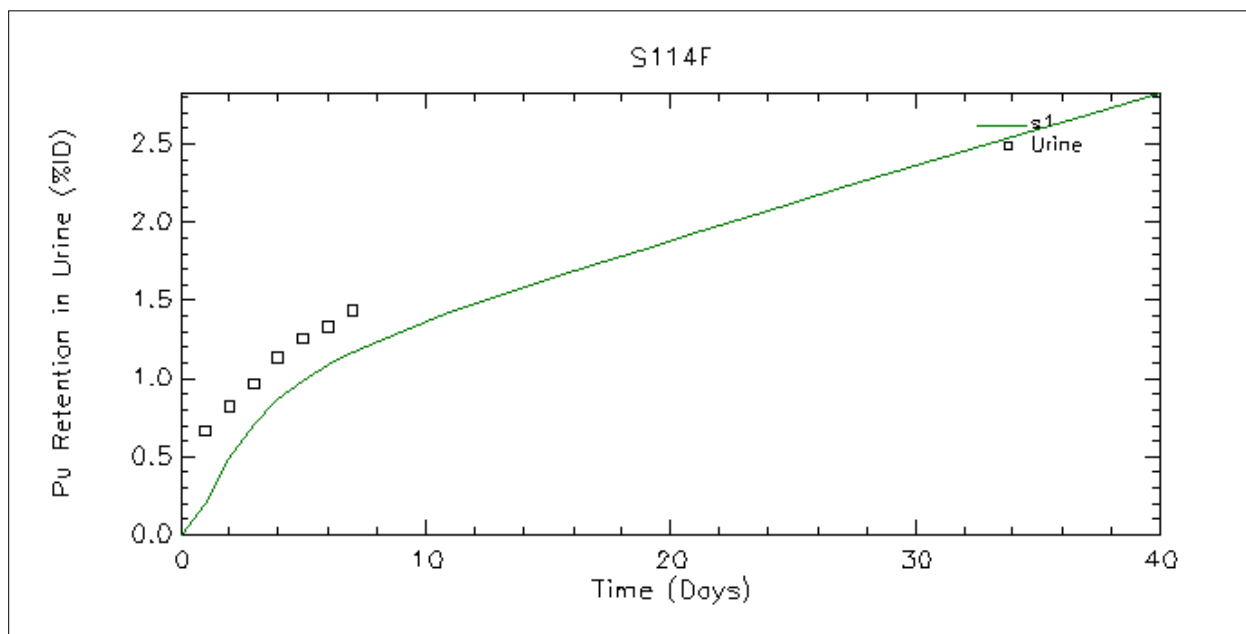


Figure 16: Case S114F sacrificed 7 days after injection

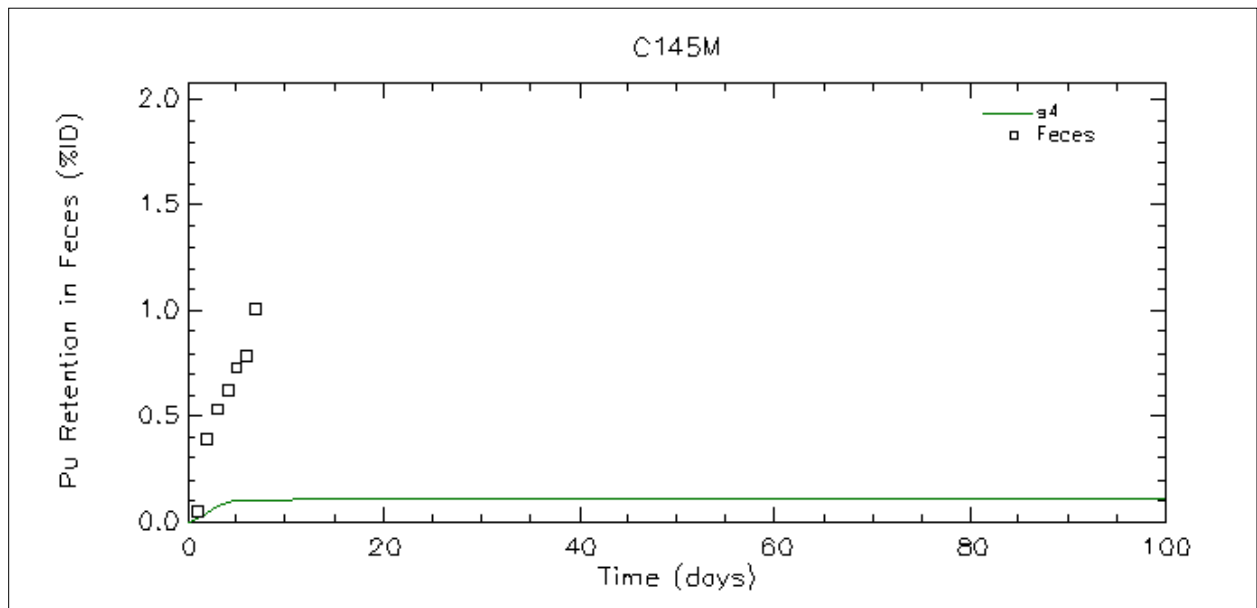
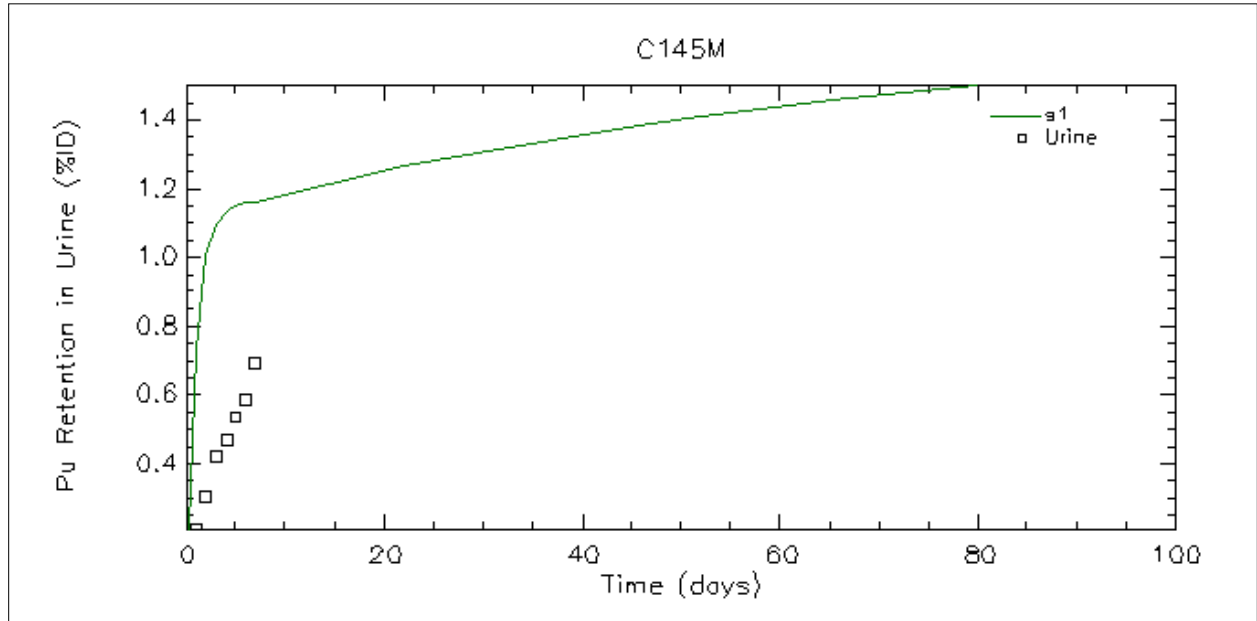


Figure 17: Case C145M sacrificed 7 days after injection

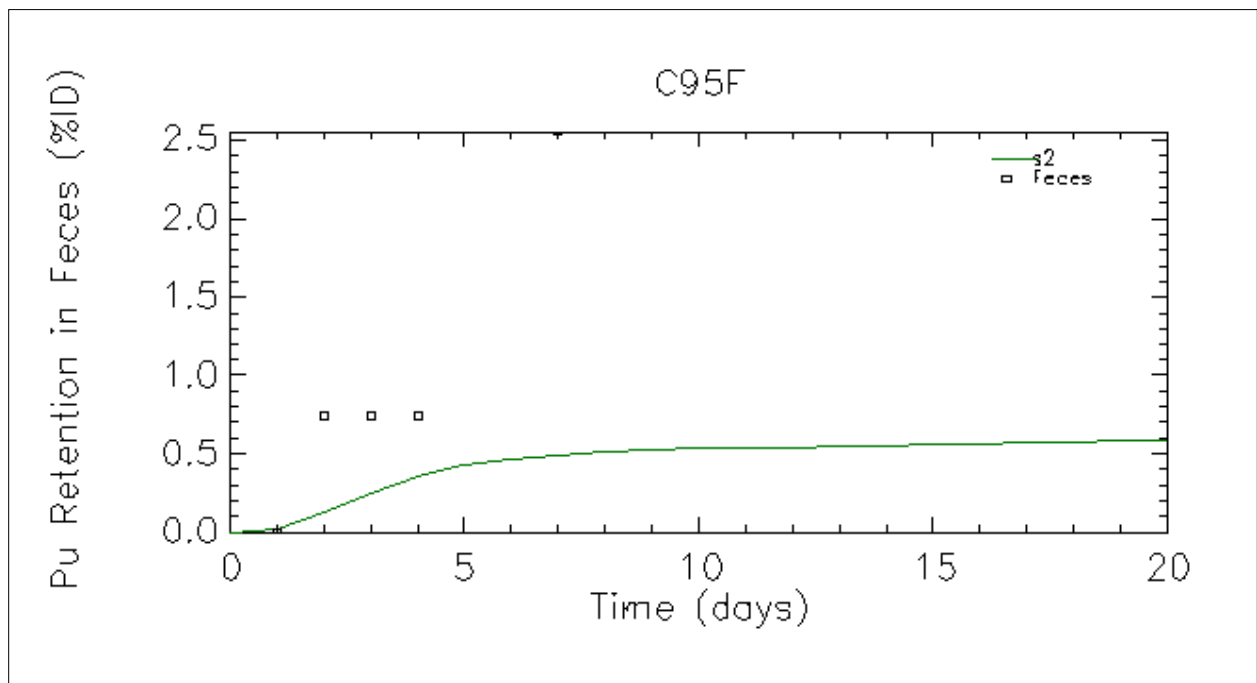
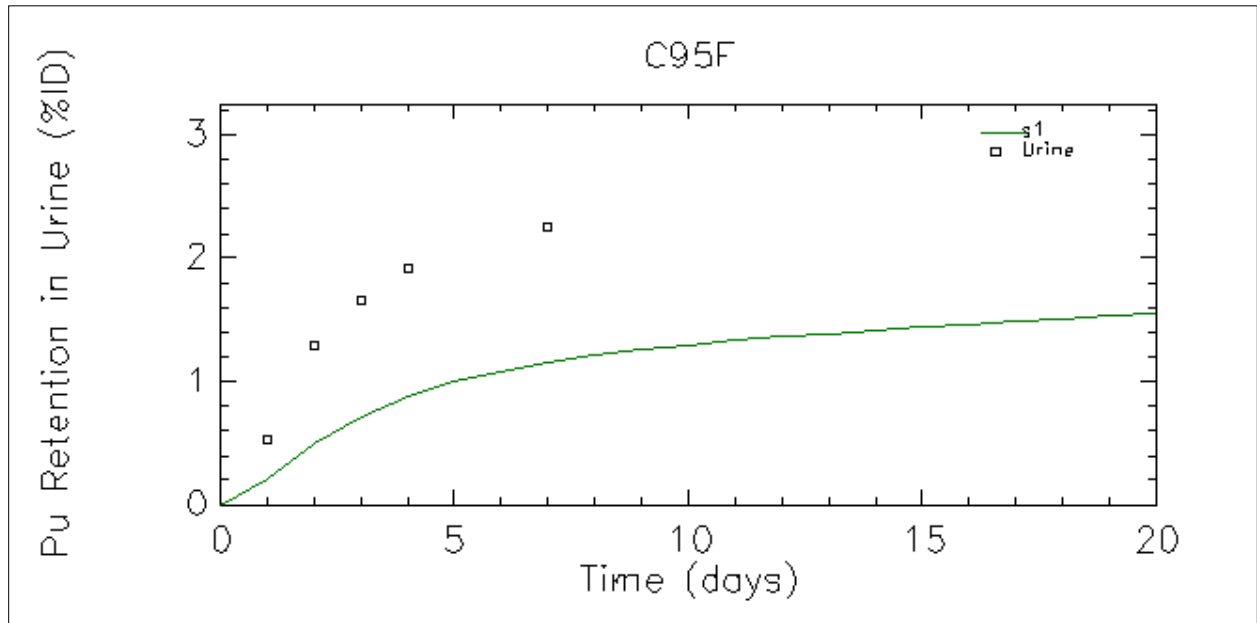


Figure 18: Case C95F sacrificed 8 days after injection

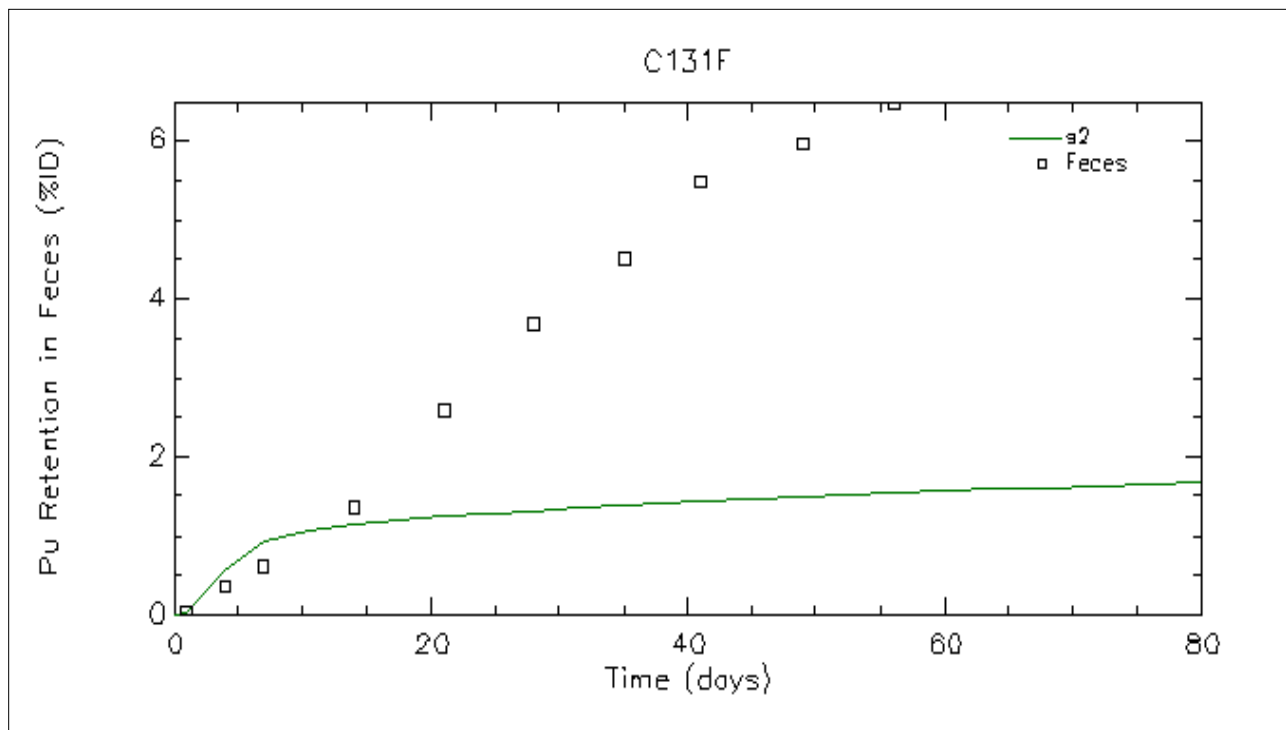
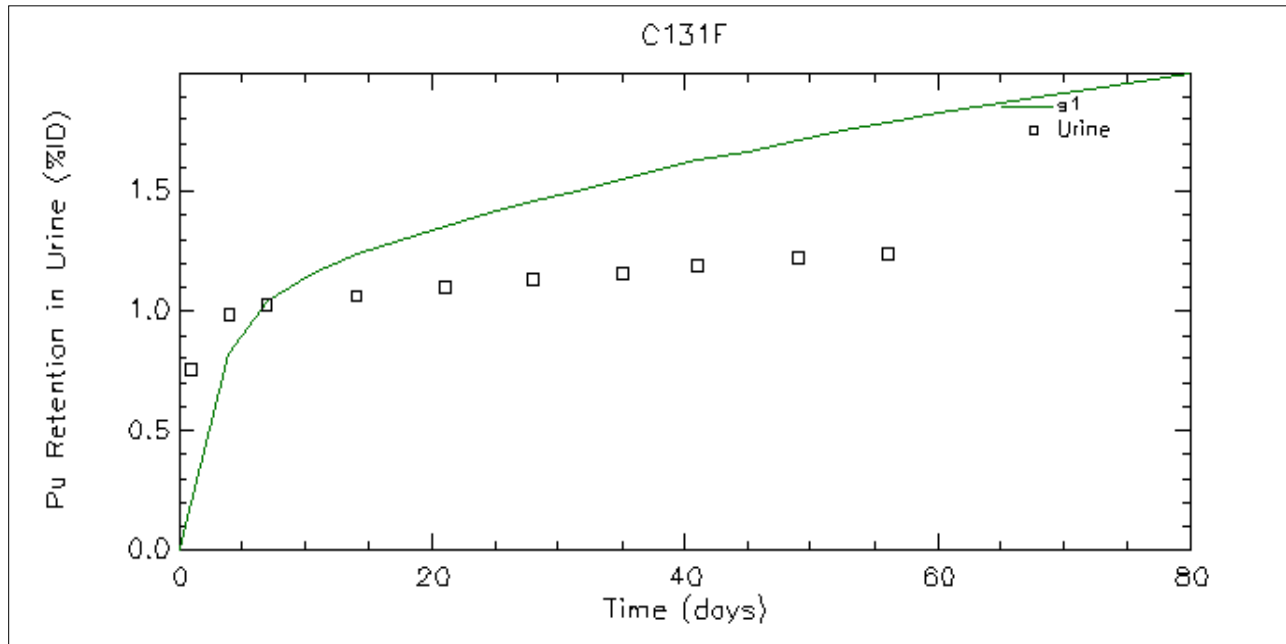


Figure 19: Case C131F sacrificed 56 days after injection

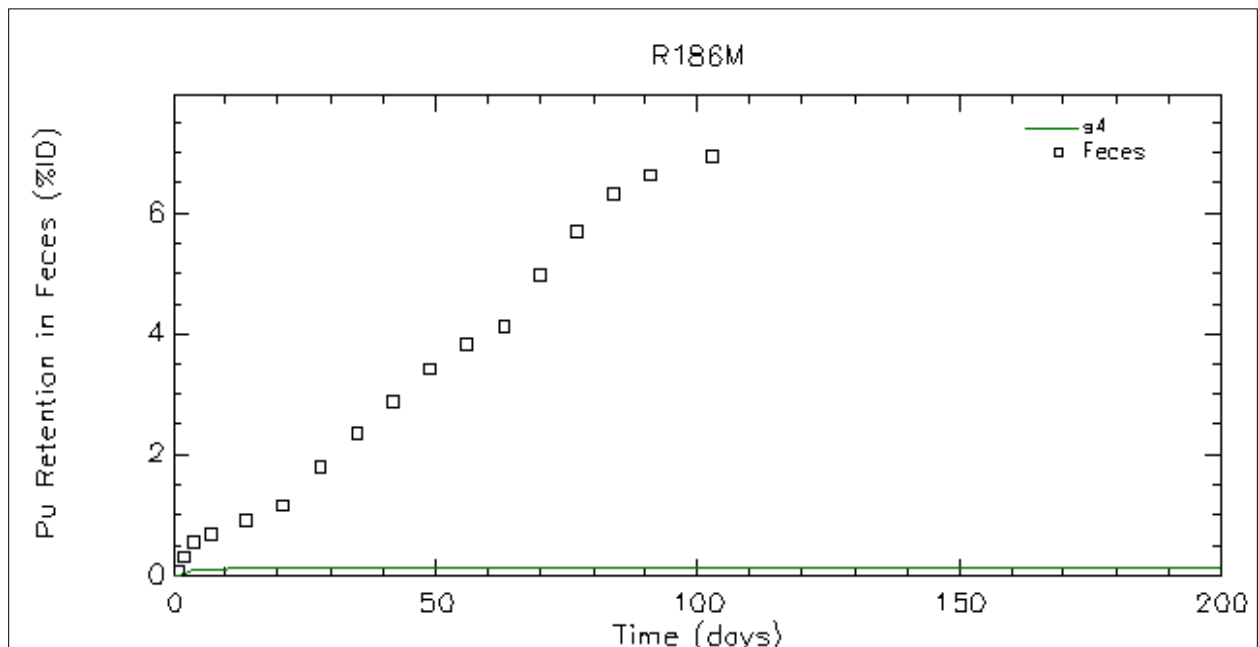
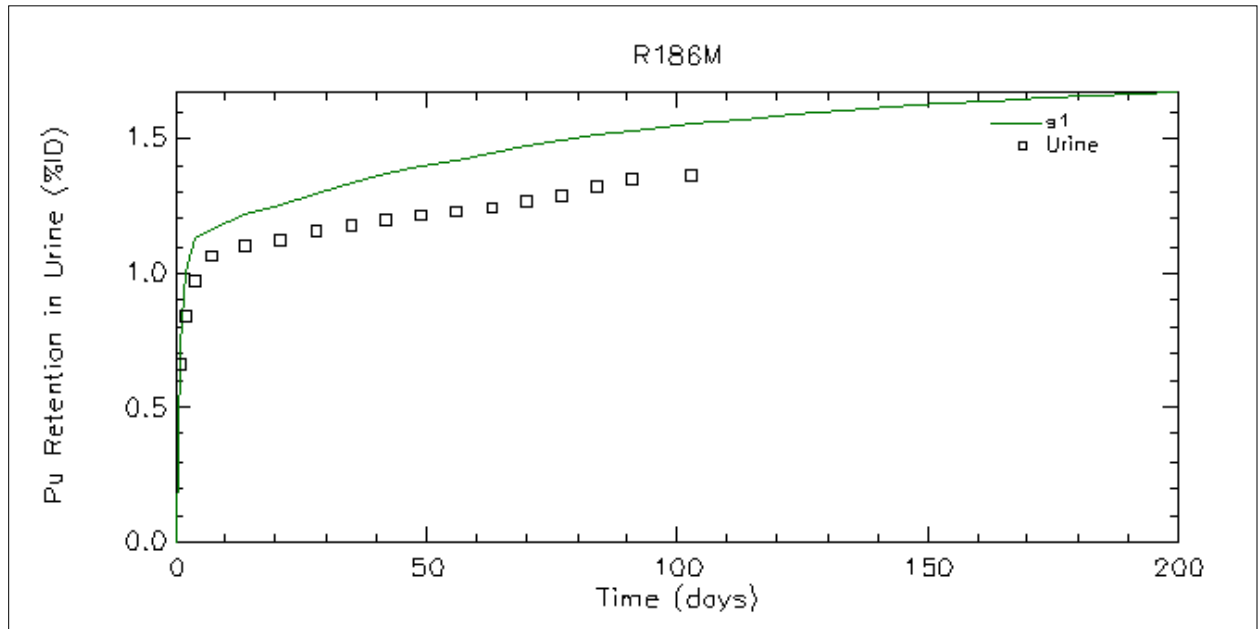


Figure 20: Case R186M sacrificed 103 days after injection

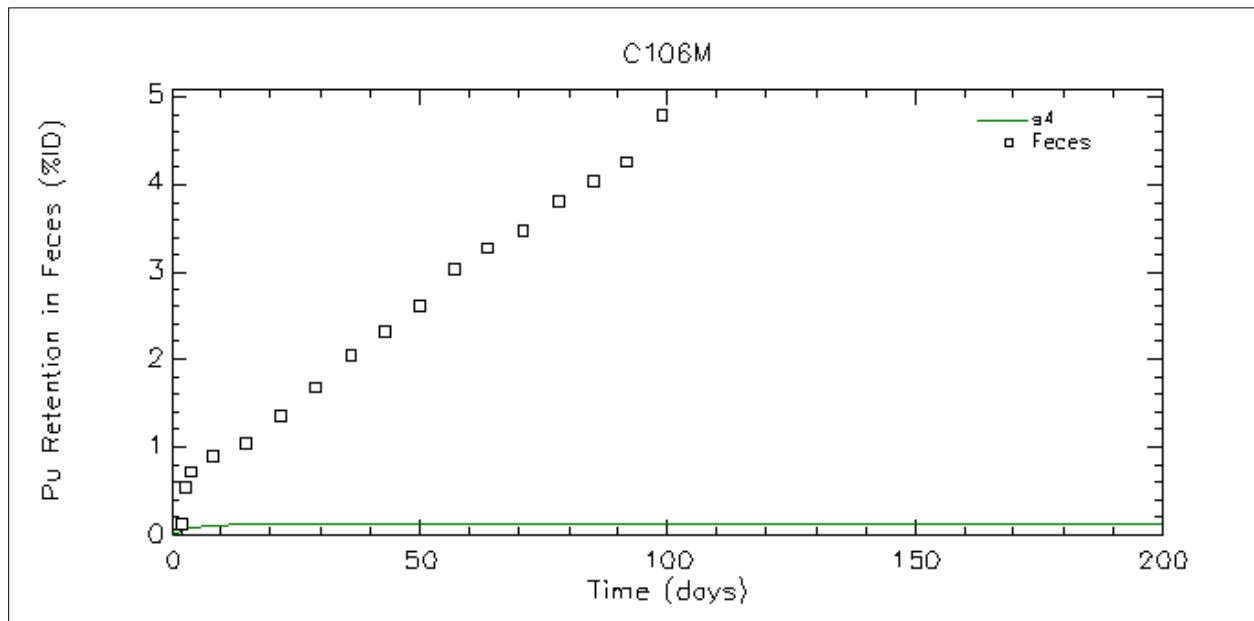
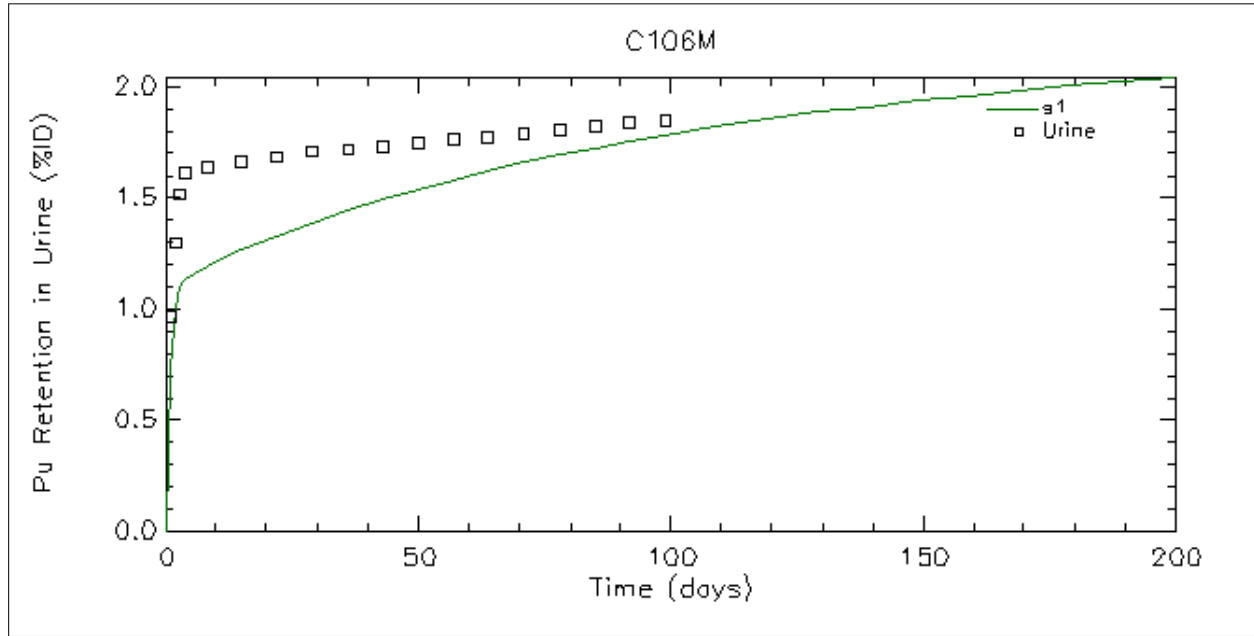


Figure 21: Case C106M sacrificed 106 days after injection

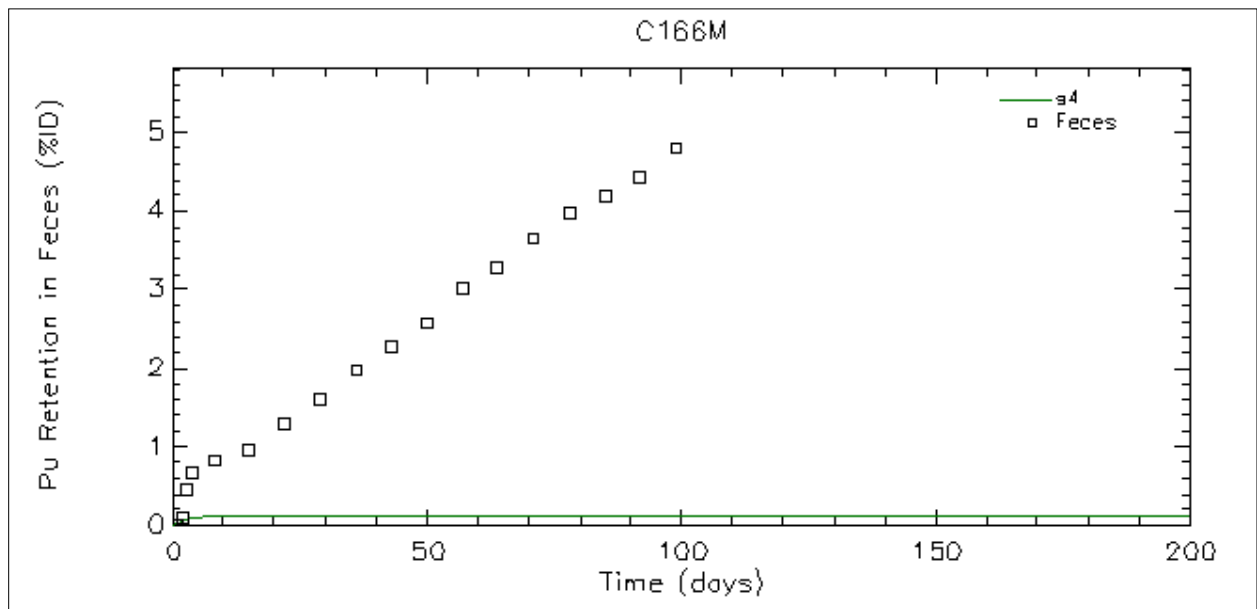
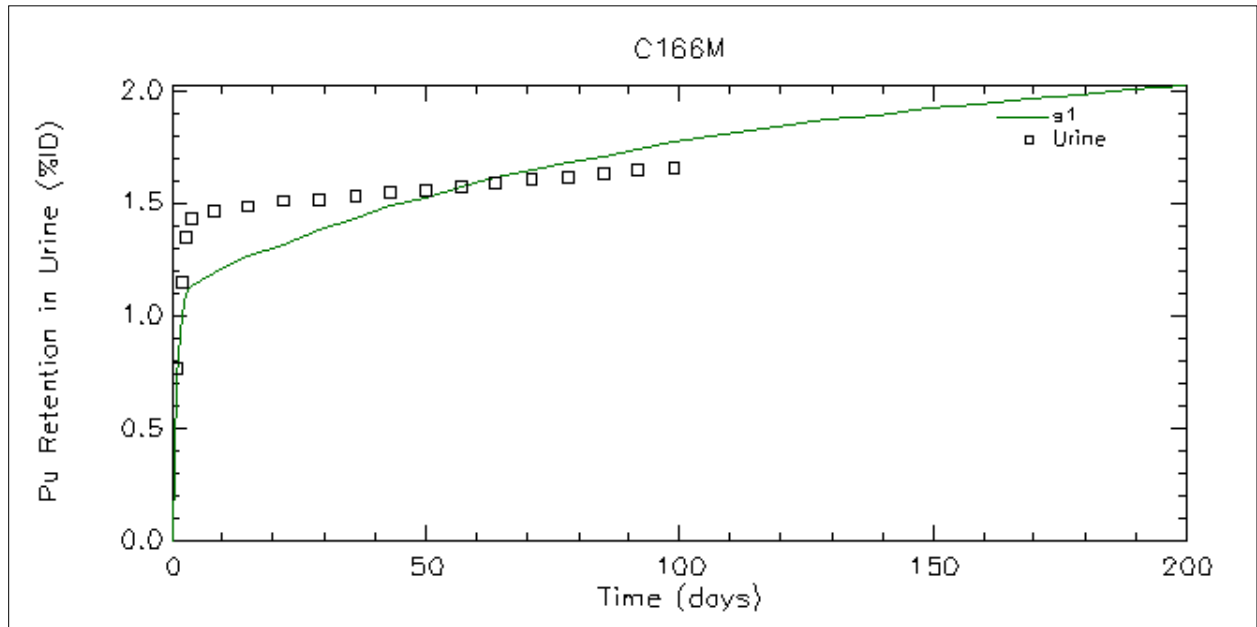


Figure 22: Case C166M sacrificed 106 days after injection

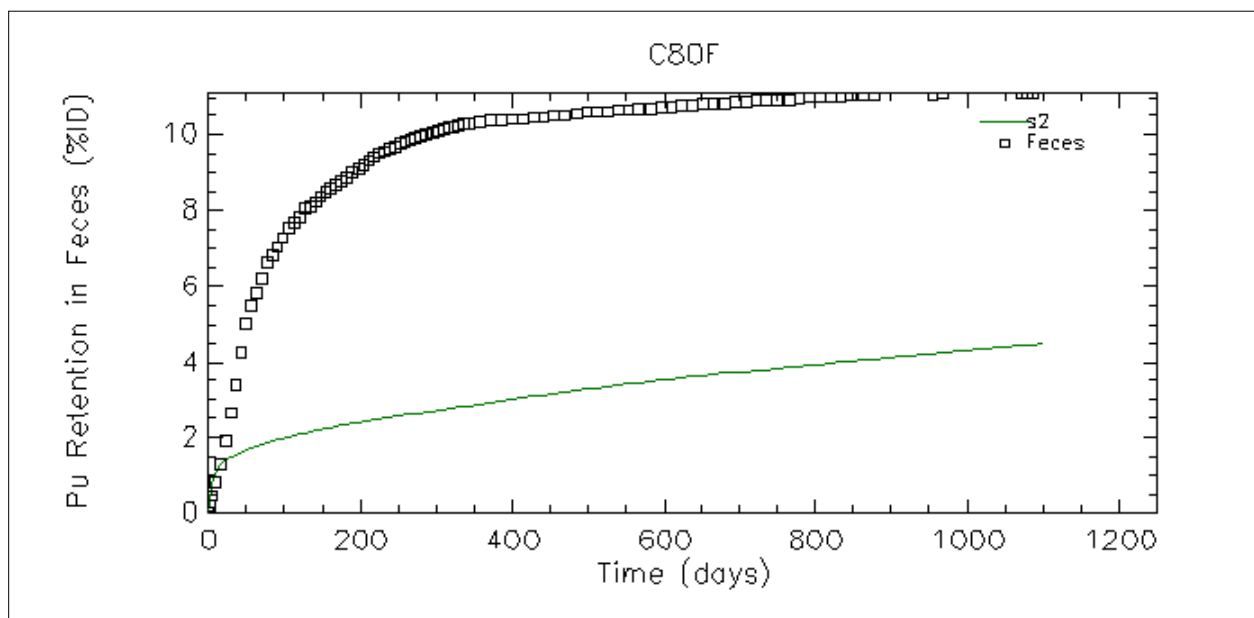
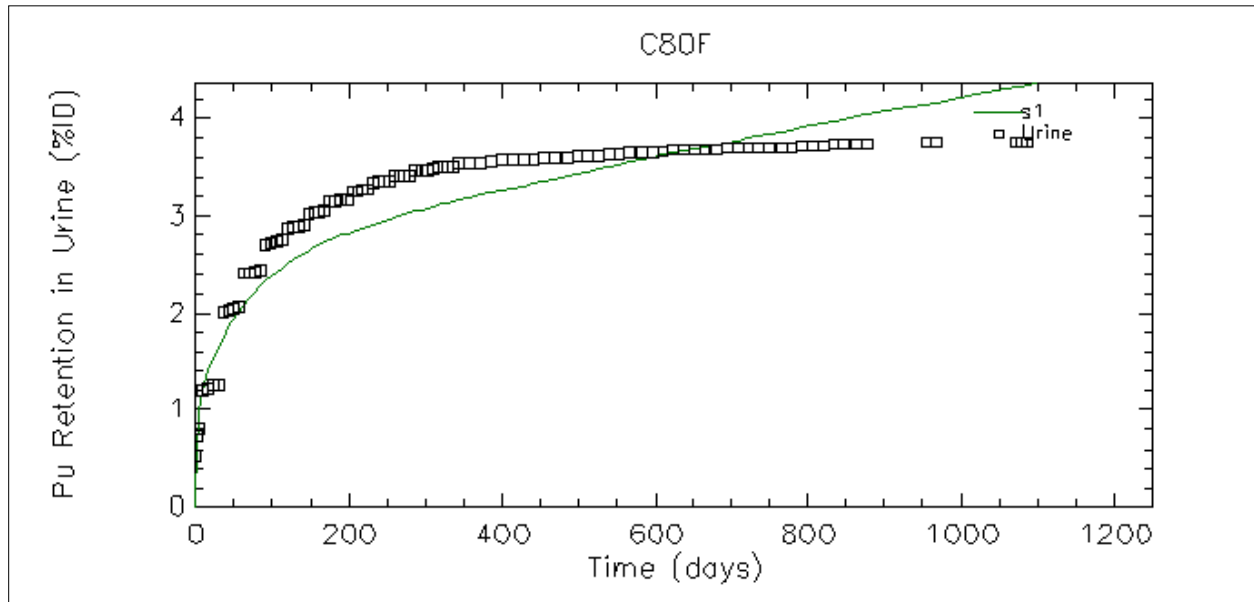


Figure 23: Case C80F sacrificed 1,100 days after injection

The solid line presents the SAAM II prediction of the activity based on the ICRP 78 systemic and the NCRP 156 wound models using the recommended default transfer rates. The data points present the bioassay measured data taken on specific days post injection. It is evident from the scatter plots demonstrated above that the plutonium retention in urine between the wound model and bioassay measurements were different. The plutonium retention in urine was lower for cases C77F (death after 2 hours post injection), C145M (death at 7 days post injection), C131F (death at 56 days post injection), and R186M (death at 103 days post injection). The plutonium retention was higher for cases C108 (death 18 hours post injection), C103F (death 20 hours post injection), and C95F (death 8 days post injection). The plutonium retention in urine for cases C106M (death 106 days post injection), C166M (death 106 days post injection), and C80F (death at 1,100 day after post injection) tended to be higher in the beginning and lower after sometime. The patterns observed when considering organ retention were similar to the wound model curve.

It is evident from the scatter plots that the plutonium concentration predicted in feces using the combined wound model and systemic model was much different than the bioassay measurements. The plutonium concentration predicted in feces was apparently higher for all cases.

The plutonium activity in liver and skeleton were predicted using the SAAM II software based upon the ICRP 78 systemic model as coupled to the NCRP 156 wound model and the recommended default transfer rates. The measured values were compared with the predicted values at the time of the autopsy. The data for measured values and the predicted values are summarized in Table 5. The proportions of the predicted values versus measured values were plotted as a function of time as shown in Figure 24. The range of the time of post injection was

from 2 hours to 1,100 days. The ratio of predicted activity in liver over the measured value at time of death is less than 1 for the primates sacrificed before 100 days except case R186M, when the fraction is 1.15. The ratio of predicted activity over measured values for case C80F is about 61, which was sacrificed at 1,100 days post injection, in this case the model over predicts the measured value by large magnitude.

The ratio of predicted activity in the skeleton over measured values was less than 1 for cases sacrificed in less than 1 day except C95F that was sacrificed 8 days after injection. The ratio is more consistent for cases sacrificed in middle and long time periods varying from 0.81 to 4.47, however, the ratio is between 0.81 and 1.93 for 7 cases out of 11. The activity in skeleton was higher than it was predicted by the model for cases sacrificed in less than 1 day. The ratio of activity in liver compared to the ratio of activity in skeleton did not show large differences for the case sacrificed at 1,100 days post injection. These results suggest that the plutonium retention in the skeleton is better described than that in the liver.

Case	Time after injection	Liver			Skeleton		
		Measured data (%ID)	SAAM Predicted	Fraction P/M	Measured data (%ID)	SAAM Predicted	Fraction P/M
C77F	2 hours	7.31	3.301	0.45	13.3	5.502	0.41
C108F	18 hours	40.6	3.301	0.08	19.0	5.502	0.29
C103F	20 hours	48.6	3.301	0.07	31.6	5.502	0.17
S114F	7 d	7.31	3.301	0.45	13.3	20.079	1.51
C145M	7 d	75.5	15.186	0.20	17.3	25.325	1.46
C95F	8 d	48.2	15.186	0.32	31.1	25.324	0.81
C131F	56 d	33.5	21.387	0.64	18.5	35.781	1.93
R186M	103 d	20.2	23.199	1.15	27.2	38.825	1.43
C166M	106 d	42.4	23.099	0.54	20.5	38.659	1.89
C106M	106 d	42	23.099	0.55	20.6	38.659	1.88
C80F	1100 d	0.47	28.782	61.24	9.89	44.214	4.47

Table 5: Summary of plutonium activity in Liver and Skeleton calculated using SAAM II and compared with the measured values at the time of autopsy.

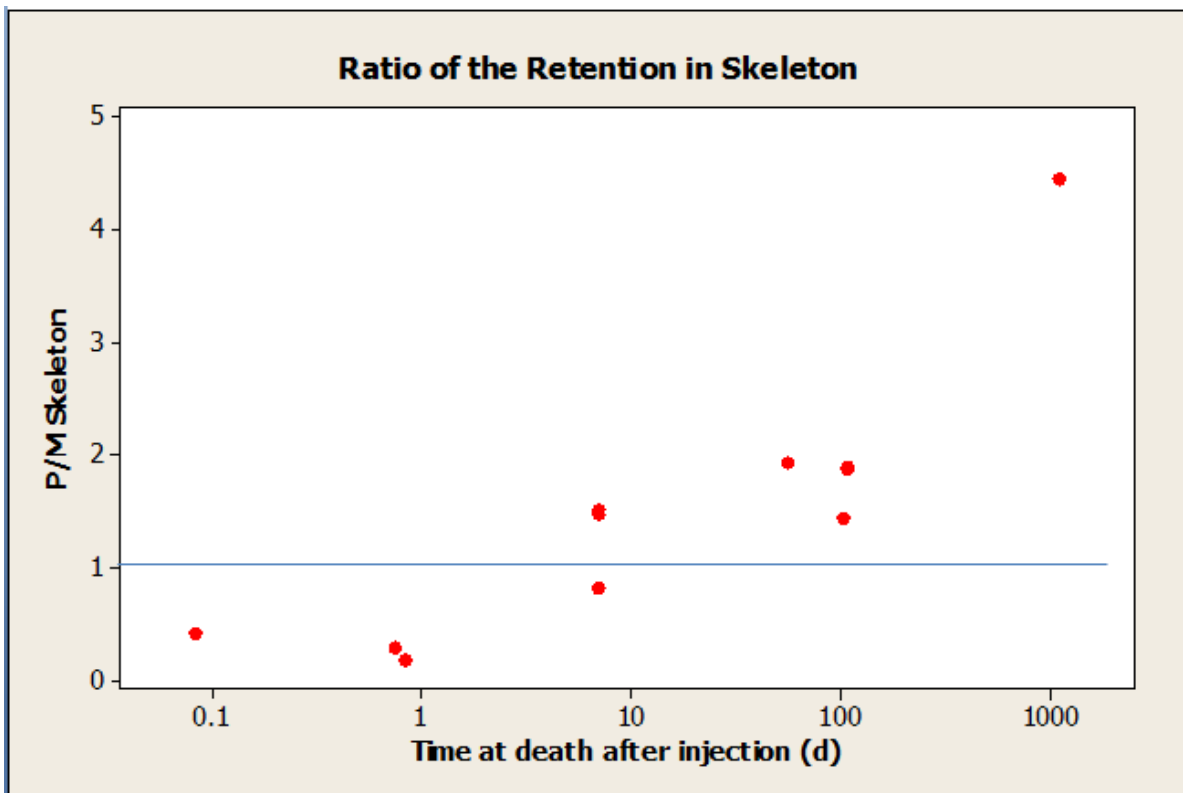
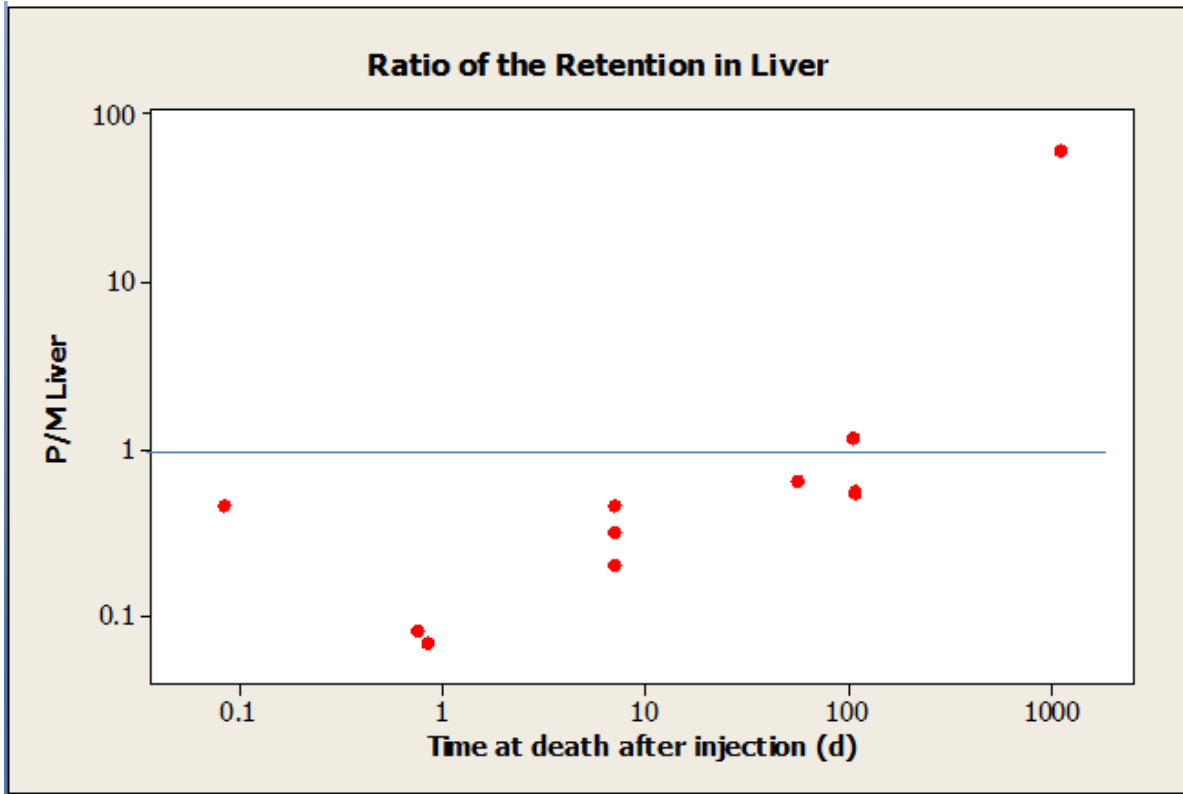


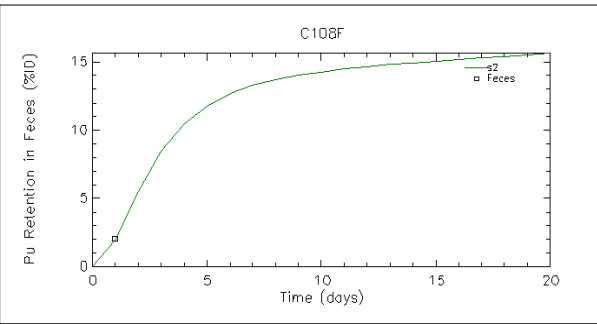
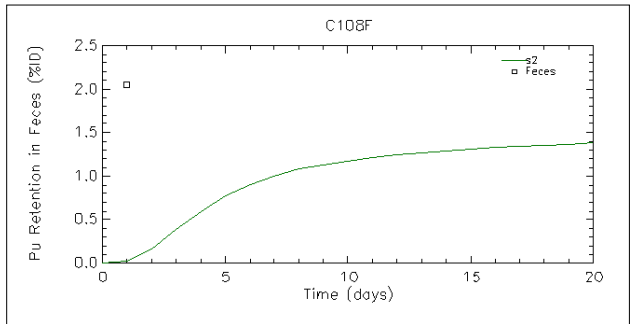
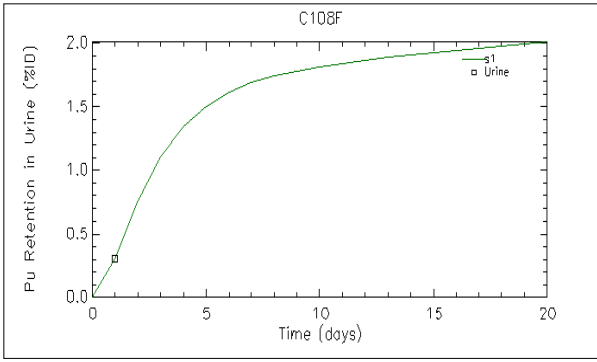
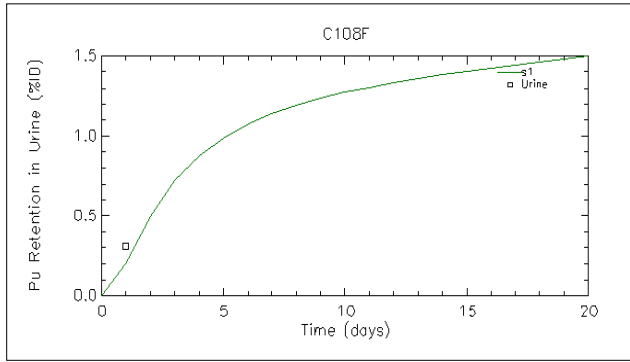
Figure 24: Scatter plots of the retention fractions in Liver and Skeleton for SAAM II prediction and measured values

4.2 Optimization of the transfer rates suggested in the ICRP 78 Systemic model and NCRP 156 Wound model for plutonium

The ICRP 78 systemic model and NCRP 156 wound model transfer rates were considered to be default transfer rates for each parameter. These parameters were used to make initial predictions for non-human primate data using SAAM II. SAAM II was also used to find the optimal values of transfer rates to improve the model fits to the data. The parameters were varied in a range between 1/10 to 10 times of the default parameters. A Bayesian method was used for the optimization of the parameters. There were 41 parameters in the systemic model when coupled to the wound model to be modified using SAAM II software. The parameters were varied by sections. The first sections that were modified were parameters that related to the soft tissue compartments and blood exchange. Then these sections were fixed and the next set of parameters related to the liver and blood exchange were varied. This procedure was repeated for all sections in the model. The last step was when all the parameters were opened for the final optimization. SAAM II calculated the values of the total objective function, AIC, and BIC, for finalized optimized version and parameters of the models investigated.

Figures 25 through 28 show a few example cases of how the fits to urine and feces data appeared when considering the default parameters recommended by ICRP 78 and NCRP 156 in contrast to the modified values. Solid lines represent the ICRP 78 and NCRP 156 predictions before employing optimized transfer rates on the graphs on the left side and after optimization transfer rates were employed on the graphs on the right side. Scattered data points represent the measured data for urine and feces.

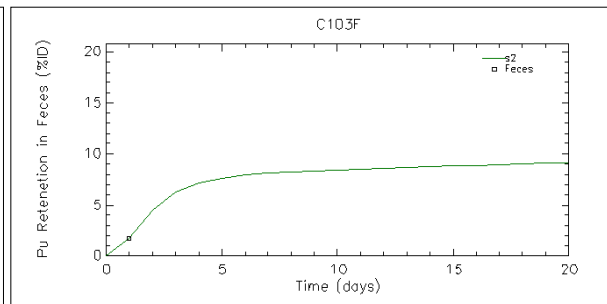
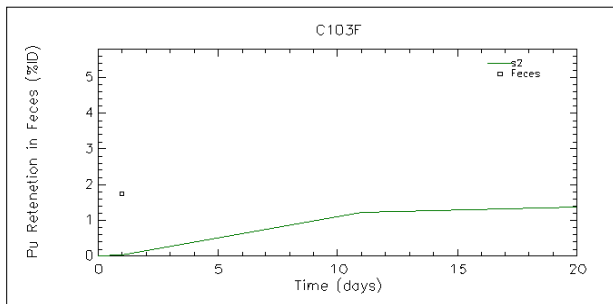
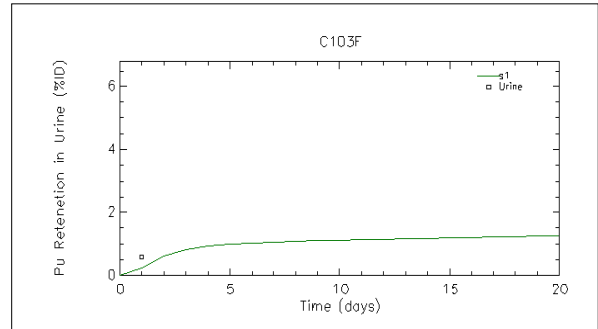
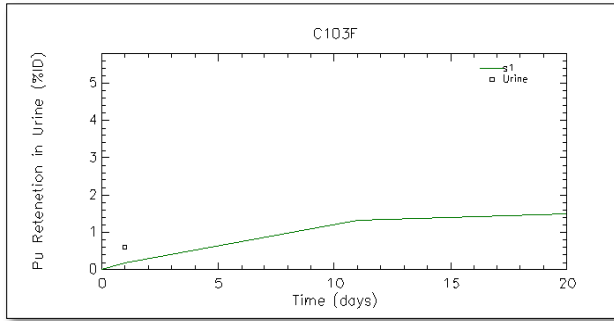
The modified transfer rates best fitting these data points generated using monkeys for the ICRP 78 systemic model and NCRP 156 wound model for plutonium are given in Table 5.



Default transfer rates

Optimized transfer rates

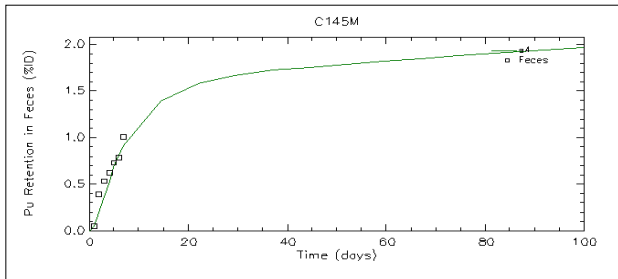
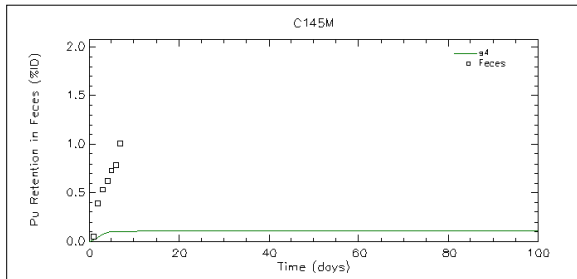
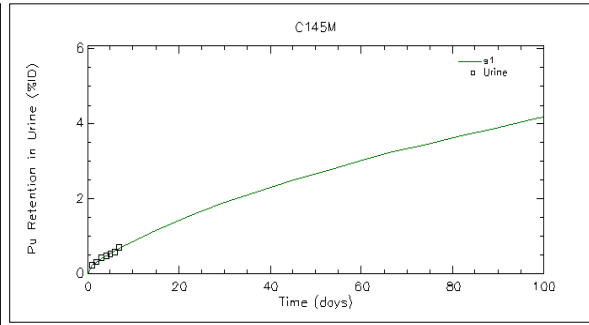
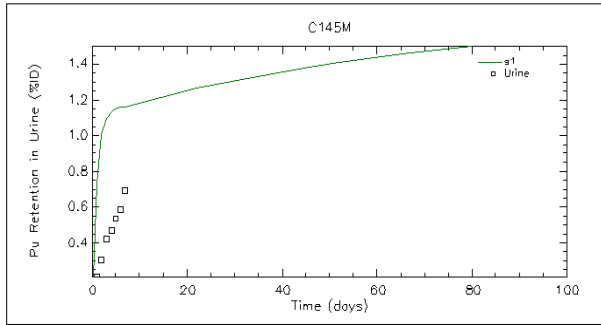
Figure 25: Case C108F sacrificed in 18 hours after injection. Initial predictions and final solutions after optimization of transfer rates.



Default transfer rates

Optimized transfer rates

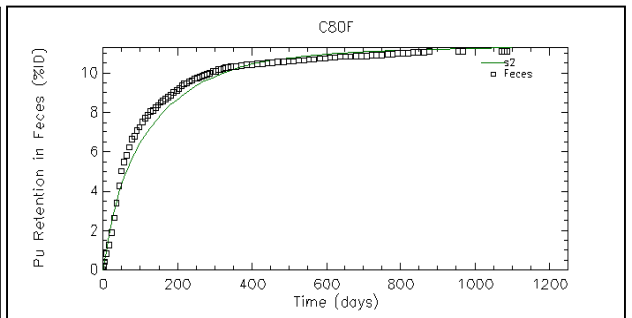
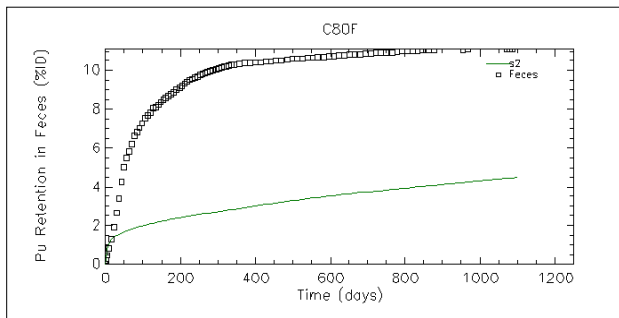
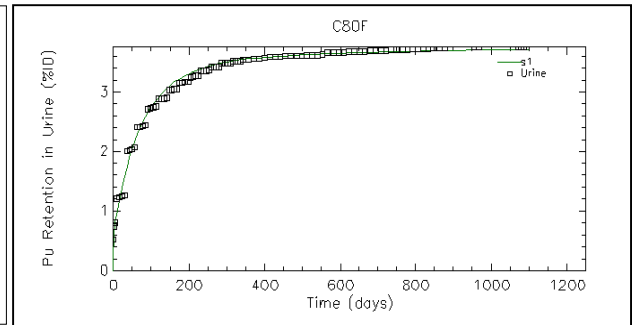
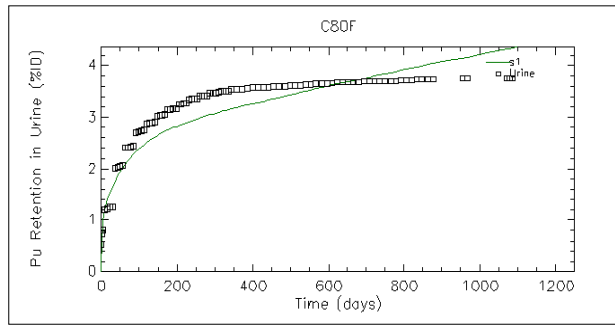
Figure 26: Case C103F sacrificed in 20 hours after injection. Initial prediction and final solution after optimization of transfer rates.



Default transfer rates

Optimized transfer rates

Figure 27: Case C145M sacrificed on 7 day after injection. Initial prediction and final solution after optimization of transfer rates.



Default transfer rates

Optimized transfer rates

Figure 28: Case C80F sacrificed on 1,100 day after injection. Initial prediction and final solution after optimization of transfer rates.

NCRP 156 & ICRP 78, Part II Continued								
From	To	Route	Default	C95F	C103F	C77F	C80F	C108F
ST0	Blood	k(1,3)	0.69300	6.76364	4.19891	3.53686	0.69300	5.77245
ST1	Blood	k(1,2)	0.00048	0.00475	0.00048	0.00048	0.00048	0.00048
ST2	Blood	k(1,4)	0.00002	0.00002	0.00002	0.00002	0.00002	0.00002
Trabecular marrow	Blood	k(1,14)	0.00760	0.00760	0.00760	0.00760	0.00760	0.00759
Cortical marrow	Blood	k(1,11)	0.00760	0.00760	0.00760	0.00760	0.00760	0.00760
Other kidney tissue	Blood	k(1,15)	0.00139	0.00139	0.00139	0.00139	0.00139	0.00140
Liver2	Blood	k(1,5)	0.00021	0.00021	0.00021	0.00021	0.00021	0.00021
Testes	Blood	k(1,8)	0.00019					
Ovaries	Blood	k(1,8)	0.00019	0.00019	0.00019	0.00019	0.00019	0.00019
Blood	ST0	k(3,1)	0.27730	0.02773	0.02773	0.02773	0.27730	0.02773
Blood	ST1	k(2,1)	0.08060	0.00806	0.00806	0.00806	0.08060	0.00806
Blood	ST2	k(4,1)	0.01290	0.00129	0.00129	0.00129	0.01290	0.00129
Blood	Trabecular surface	k(13,1)	0.19410	0.19434	0.19381	0.19410	0.19410	0.19229
Blood	Cortical surface	k(10,1)	0.12940	0.12951	0.12927	0.12940	0.12940	0.12893
Trabecular surface	Trabecular volume	k(12,13)	0.00025	0.00025	0.00025	0.00025	0.00025	0.00025
Cortical surface	Cortical volume	k(9,10)	0.00004	0.00004	0.00004	0.00004	0.00004	0.00004
Trabecular surface	Trabecular marrow	k(14,13)	0.00049	0.00049	0.00049	0.00049	0.00049	0.00049
Trabecular volume	Trabecular marrow	k(14,12)	0.00049	0.00049	0.00049	0.00049	0.00049	0.00049
Cortical surface	Cortical marrow	k(11,10)	0.00008	0.00008	0.00008	0.00008	0.00008	0.00008
Cortical volume	Cortical marrow	k(11,9)	0.00008	0.00008	0.00008	0.00008	0.00008	0.00008
Blood	Other kidney tissue	k(15,1)	0.00323	0.00315	0.00319	0.00323	0.00323	0.00032
Blood	Liver1	k(6,1)	0.19410	0.14323	0.38801	0.19410	0.19410	0.01941
Liver1	Liver2	k(5,6)	0.00177	0.00175	0.00177	0.00177	0.00177	0.00177
Blood	Testes	k(8,1)	0.00023					
Blood	Ovaries	k(8,1)	0.00007	0.00007	0.00007	0.00007	0.00007	0.00001
Liver1	Small intestine	k(7,6)	0.00013	0.00037	0.00019	0.00013	0.00013	0.00015
Blood	Upper large intestine	k(18,1)	0.01290	0.04468	0.12896	0.01290	0.01290	0.12900
Blood	Urinary path	k(16,1)	0.00647	0.00065	0.00640	0.00647	0.00647	0.00065
Blood	Bladder	k(17,1)	0.01290	0.02567	0.01664	0.00129	0.01290	0.01624
ST1	Bladder	k(17,2)	0.00048	0.00475	0.00075	0.00005	0.00048	0.00158
Urinary path	Bladder	k(17,16)	0.01386	0.00139	0.01391	0.01386	0.01386	0.01600
SI	ULI	k(18,7)	6.00000	9.83945	7.17585	6.00000	6.00000	6.41073
ULI	LLI	k(19,18)	1.80000	0.19865	17.99944	0.18000	1.80000	18.00000
LLI	Feces	k(20,19)	1.00000	0.15327	9.99945	0.10000	1.00000	10.00000
Bladder	Urine	k(21,17)	12.00000	76.01705	13.66023	12.00000	12.00000	120.00000
Soluble	Blood	k(1,22)	0.67000	0.67000	0.67047	1.42430	0.67000	0.67551
Soluble	CIS	k(23,22)	0.60000	0.60000	0.59782	0.06000	0.60000	0.62417
CIS	Soluble	k(22,23)	0.02400	0.02400	0.02400	0.02400	0.02400	0.02399
CIS	PABS	k(24,23)	0.00970	0.00970	0.00970	0.00967	0.00970	0.00970
PABS	Soluble	k(22,24)	0.00120	0.00120	0.00120	0.00120	0.00120	0.00120
PABS	Lymph nodes	k(25,24)	0.00002	0.00002	0.00002	0.00002	0.00002	0.00002
Lymph nodes	Blood	k(1,25)	0.02900	0.02900	0.02900	0.02900	0.02900	0.02900

Table 6: Summary for the modified transfer rates for each case

The calculation of Geometric mean and Geometric Standard Deviation (GSD) for each of the optimized parameters considered for all animals in the study ICRP 78 systemic model and NCRP 156 wound model parameter was completed. The GSD values are significant for evaluation of the range of modified transfer rates in the region of average geometric mean. The values are provided in Table 7.

	NCRP 156 & ICRP 78		Default	Geom Mean	GSD
ST0	Blood	k(1,3)	0.69300	2.12320	4.63447
ST1	Blood	k(1,2)	0.00048	0.00031	4.70049
ST2	Blood	k(1,4)	0.00002	0.00001	2.45877
Trabecular marrow	Blood	k(1,14)	0.00760	0.00760	2.66692
Cortical marrow	Blood	k(1,11)	0.00760	0.00724	2.00381
Other kidney tissue	Blood	k(1,15)	0.00139	0.00078	2.83255
Liver2	Blood	k(1,5)	0.00021	0.00017	1.93867
Testes	Blood	k(1,8)	0.00019	0.00019	1.04470
Ovaries	Blood	k(1,8)	0.00019	0.00019	1.01142
Blood	ST0	k(3,1)	0.27730	0.06692	3.90971
Blood	ST1	k(2,1)	0.08060	0.02371	4.11865
Blood	ST2	k(4,1)	0.01290	0.00408	6.27629
Blood	Trabecular surface	k(13,1)	0.19410	0.19007	1.17427
Blood	Cortical surface	k(10,1)	0.12940	0.10540	1.93872
Trabecular surface	Trabecular volume	k(12,13)	0.00025	0.00020	1.94352
Cortical surface	Cortical volume	k(9,10)	0.00004	0.00004	1.00336
Trabecular surface	Trabecular marrow	k(14,13)	0.00049	0.00049	2.66710
Trabecular volume	Trabecular marrow	k(14,12)	0.00049	0.00050	1.08902
Cortical surface	Cortical marrow	k(11,10)	0.00008	0.00008	2.12488
Cortical volume	Cortical marrow	k(11,9)	0.00008	0.00008	1.00090
Blood	Other kidney tissue	k(15,1)	0.00323	0.00439	3.31836
Blood	Liver1	k(6,1)	0.19410	0.19669	2.51033
Liver1	Liver2	k(5,6)	0.00177	0.00144	1.95228
Blood	Testes	k(8,1)	0.00023	0.00010	2.37110
Blood	Ovaries	k(8,1)	0.00007	0.00006	2.52850
Liver1	Small intestine	k(7,6)	0.00013	0.00025	2.89992
Blood	Upper large intestine	k(18,1)	0.01290	0.01603	4.32932
Blood	Urinary path	k(16,1)	0.00647	0.00229	3.14559
Blood	Bladder	k(17,1)	0.01290	0.01269	2.12221
ST1	Bladder	k(17,2)	0.00048	0.00054	5.69261
Urinary path	Bladder	k(17,16)	0.01386	0.00621	3.06615
SI	ULI	k(18,7)	6.00000	6.80712	2.59232
ULI	LLI	k(19,18)	1.80000	1.68917	4.77161
LLI	Feces	k(20,19)	1.00000	0.76118	5.27707
Bladder	Urine	k(21,17)	12.00000	34.56387	3.02516
Soluble	Blood	k(1,22)	0.67000	0.68562	1.30938
Soluble	CIS	k(23,22)	0.60000	0.44273	2.10607
CIS	Soluble	k(22,23)	0.02400	0.00941	5.93671
CIS	PABS	k(24,23)	0.00970	0.01175	1.94405
PABS	Soluble	k(22,24)	0.00120	0.00209	3.17791
PABS	Lymph nodes	k(25,24)	0.00002	0.00002	1.70370
Lymph nodes	Blood	k(1,25)	0.02900	0.02494	1.68685

Table 7: Geometric mean and GSD values with default parameters published in ICRP 78 & NCRP

The value for the total objective function corresponds to AIC statistics for each particular case. The AIC statistics was used to compare the default and optimized models with each other. Based on Table 8 only four cases S114F, C145M, R186M and C80F gave lower AIC values, meaning better statistical fit, for default model while the rest of the seven cases gave lower AIC values for optimized model, therefore making the optimized model preferential for monkey data.

Case	Total objective function default	Total objective function optimized	AIC _{default}	AIC _{optimized}
C77F	-1.185	-1.867	1.326	0.985
C108F	1.470	-1.542	2.654	1.147
C103F	3.367	1.200	3.603	1.310
S114F	-1.469	-1.880	0.479	0.760
C145M	-1.416	-2.360	0.505	0.520
C95F	1.100	-1.530	1.854	0.990
C131F	0.263	-1.390	1.268	0.930
R186M	0.355	0.080	1.232	1.540
C166M	6.150	0.307	4.122	1.640
C106M	6.313	-1.240	4.204	-0.810
C80F	1.963	2.920	1.927	2.570

Table 8: Total objective function values and corresponding AICs

The exponential expression can be calculated as $exp^{(-\frac{\Delta_i}{2})}$ where Δ_i represents the AIC differences, determining which of these models best describes the data. Table 9 below summarizes these values.

Case	$\exp(-1/2*\Delta i)$
C77F	0.843
C108F	0.471
C103F	0.318
S114F	1.151
C145M	1.007
C95F	0.649
C131F	0.845
R186M	1.167
C166M	0.289
C106M	0.082
C80F	1.380

Table 9: Exponential function values

Case	Optimized model likelihood	Default model likelihood
C77F	1.186	0.843
C108F	2.125	0.471
C103F	3.146	0.318
S114F	0.869	1.151
C145M	0.993	1.007
C95F	1.540	0.649
C131F	1.184	0.845
R186M	0.857	1.167
C166M	3.459	0.289
C106M	12.269	0.082
C80F	0.725	1.380

Table 10: Likelihood of each model based on exponential function

Exponential function in Table 9 varies between 0.081 and 1.379 for different cases. All the values are relatively close to one. In four cases C80F, R186M, C145M and S114F the exponential function values are bigger than one. Therefore, for the rest of the seven cases the exponential function values are less than one. This means the default model is a better fit for the four cases which had exponential value bigger than one, whereas the optimized model is a better fit for the seven cases that have exponential values less than one.

Based on Table 10 it can be concluded that optimized model is a better fit than the default model for most of the cases. In three cases C103F, C166M and C106M the optimal model was better by a margin of at least 3 to 1, in the other cases both models fit about equally well.

Since all the AIC values are relatively close to one, therefore it is hard to make either model default or optimized, preferential over the other, cause the values are based on the few available non-human primate population.

Chapter 5

SUMMARY AND CONCLUSIONS

5.1. Summary of Results

The predictions of the default transfer rates of the NCRP 156 wound model coupled to ICRP 78 systemic model for Pu-238 do not coincide with the measurement values of Pu concentration in excreta or liver and skeleton tissue sample activity measurements at time of death. The predicted values in most cases were evaluated to be lower than the bioassay measurement values for the concentration of Pu-238 in urine and feces. The ratio of predicted activity in liver over the measured value at time of death is less than 1 for the 7 primates sacrificed before 100 days, except in one case. This same ratio for the 1 case that sacrificed at 1,100 day of post injection was about 61.

The plutonium activity predicted in skeleton compared to measured values was more consistent for cases sacrificed in middle (7 to 106 days) and long time (1,100 days) periods varying from 0.81 to 4.47, however, the ratio is most frequently observed were between 0.81 and 1.93 for 7 cases out of 11. The ratio of activity in the liver compared to the ratio of activity in skeleton was not that large, the results based on the model for the plutonium retention in the skeleton was better characterized than that in liver. The range for the ratio of activity in the liver is 0.07 to 61, whereas the range of the ratio of activity in skeleton is 0.17 to 4.47.

The optimization of the transfer rates of the NCRP 156 default wound model coupled to the ICRP 78 default systemic model was attempt to obtain better fits to the bioassay data. The retention predictions of the optimized parameters in excretion were higher than those obtained using default model parameters. The predictions based on optimized transfer rates in the liver and skeleton showed improvement for many, but not for all cases.

5.2 Future work

Biological parameters like the ones investigated during this project demonstrate considerable variability. The animals used in the Durbin experiments were physiologically close to humans. This observation supports their application as alternatives to the transfer rates published in the ICRP 78 and NCRP 156. Normalizing the Durbin results to account for the mass and size of the tissues combined with the age and life-time of the test animals could give a better understanding of the metabolic behavior that should be anticipated in humans.

Data sets that more closely consider the biochemical end points of the radioactive materials measured in organs and excreta could be of great value to better understanding and predicting the translocation of radioactive materials in humans.

References:

1. Guilmettel RA, Hickmanz AW, Fl G. To be published in the Proceedings of the International 8th Congress,. 1992;(May).
2. Burnham, K.A., Anderson, D.R. (2002). Model selection and multimodel inference: a practical information-theoretic approach. New York: Springer-Verlag.
3. Lee D. PLUTONIUM FECAL AND URINARY EXCRETION FUNCTIONS : DERIVATION FROM A SYSTEMIC WHOLE-BODY RETENTION FUNCTION Compartmental Analysis and a Generalized Mammillary Model Proposed Model for Assessing Plutonium Content in Feces. 1996;(1):1–12.
4. Phan G, Le Gall B, Deverre J-R, Fattal E, Bénech H. Predicting plutonium decorporation efficacy after intravenous administration of DTPA formulations: Study of pharmacokinetic-pharmacodynamic relationships in rats. *Pharm. Res.* 2006;23(9):2030–5. Available at: <http://www.ncbi.nlm.nih.gov/pubmed/16951998>. Accessed July 23, 2014.
5. Luciani a, Doerfel H, Polig E. Sensitivity analysis of the urinary excretion of plutonium. *Radiat. Prot. Dosimetry.* 2001;93(2):179–83. Available at: <http://www.ncbi.nlm.nih.gov/pubmed/11548342>.
6. Fritsch P, Grappin L, Guillermin AM, et al. MODELLING OF BIOASSAY DATA FROM A P U WOUND TREATED BY REPEATED DTPA PERFUSIONS : BIODYNAMICS AND. 2007;127(1):120–124.
7. Schimmelpfeng J. Physiology-based modelling in radiation research: the biokinetics of plutonium. *Radiat. Prot. Dosimetry.* 2009;136(2):74–81. Available at: <http://www.ncbi.nlm.nih.gov/pubmed/19689951>.
8. Suslova KG, Khokhryakov VF, Sokolova AB, Miller SC. 238Pu. *Health Phys.* 2012;102(3):251–262. Available at: <http://content.wkhealth.com/linkback/openurl?sid=WKPTLP:landingpage&an=00004032-201203000-00002>. Accessed July 23, 2014.
9. Miller G, Martz HF, Little TT, Guilmette R. BAYESIAN INTERNAL DOSIMETRY CALCULATIONS USING. 2002;98(2):191–198.

10. Be P. REVIEW OF METHODS AND COMPUTER CODES FOR. 2003;105:341–346.
11. W. Leggett R. Reliability of the ICRP’s dose coefficients for members of the public: US Government III. Plutonium as a case study of uncertainties in the systemic biokinetics of radionuclides. *Radiat. Prot. Dosimetry*. 2003;106(2):103–120. Available at: <http://rpd.oxfordjournals.org/cgi/doi/10.1093/oxfordjournals.rpd.a006340>.
12. Miller G, Riddell a E, Filipy R, Bertelli L, Little T, Guilmette R. Worldwide bioassay data resources for plutonium/ameridium internal dosimetry studies. *Radiat. Prot. Dosimetry*. 2007;125(1-4):531–7. Available at: <http://www.ncbi.nlm.nih.gov/pubmed/17337740>. Accessed July 23, 2014.
13. Birchall A, Puncher M, Harrison J, et al. Plutonium worker dosimetry. *Radiat. Environ. Biophys*. 2010;49(2):203–12. Available at: <http://www.ncbi.nlm.nih.gov/pubmed/20131061>. Accessed July 23, 2014.
14. Klein W, Breustedt B. Analysis of the effects of inter-individual variation in the distribution of plutonium in skeleton and liver. *Radiat. Prot. Dosimetry*. 2014;158(3):276–84. Available at: <http://www.ncbi.nlm.nih.gov/pubmed/24114619>.
15. Puncher M, Birchall A, Bull RK. AN INTAKE PRIOR FOR THE BAYESIAN ANALYSIS OF PLUTONIUM AND URANIUM EXPOSURES IN AN. 2013:1–10.
16. Suslova KG, Sokolova AB, Khokhryakov V V., Miller SC. 238Pu. *Health Phys*. 2012;102(3):243–250. Available at: <http://content.wkhealth.com/linkback/openurl?sid=WKPTLP:landingpage&an=00004032-201203000-00001>. Accessed July 23, 2014.
17. Wakeford R. More on the risk of cancer among nuclear workers. *J. Radiol. Prot*. 2009;29(1):1–4. Available at: <http://www.ncbi.nlm.nih.gov/pubmed/19229102>. Accessed July 23, 2014.
18. Stebbings JH. A case study of selected medical findings among plutonium injectees. *Health Phys*. 1999;76(5):477–88. Available at: <http://www.ncbi.nlm.nih.gov/pubmed/10201560>.
19. Sato H, Yamada Y, Ishigure N, et al. Retention, excretion and translocation of 239Pu in rats following inhalation of 239PuO₂ calcined at 1150 and 400 degrees C. *J. Radiat.*

- Res.* 1999;40(2):197–204. Available at:
<http://www.ncbi.nlm.nih.gov/pubmed/10494150>.
20. Sokolnikov ME, Gilbert ES, Preston DL, et al. Lung, liver and bone cancer mortality in Mayak workers. *Int. J. Cancer.* 2008;123(4):905–11. Available at:
<http://www.pubmedcentral.nih.gov/articlerender.fcgi?artid=4020282&tool=pmcentrez&rendertype=abstract>. Accessed July 23, 2014.
 21. Durbin, P.W. *et al.* (1990). *Collected original data on distribution of Pu-238 in soft tissues and bones of monkeys*. Lawrence Berkley Laboratory report LBL-28648.
 22. International Commission on Radiological Protection. (1993).
 23. *ICRP Publication 67; Ann ICRP 23(3-4)*. New York: Pergamon Press.
 24. Leggett RW, A Model of the Retention, Translocation and Excretion of Systemic Pu, *Health Phys*, vol. 49, pp. 1115–1137, 1985.
 25. Radiation Protection. (2012, March 6). Retrieved June 14, 2014, from
<http://www.epa.gov/radiation/radionuclides/plutonium.html>
 26. Physical, Nuclear, and Chemical Properties of Plutonium. (2012, April 10). Retrieved June 14, 2014, from <http://ieer.org/resource/nuclear-power/plutonium-factsheet/>